Titanium isotope fractionation in solar system materials

Chemical Geology 568 (2021) 120009

Contents lists available at ScienceDirect

Chemical Geology

journal homepage: www.elsevier.com/locate/chemgeo

Titanium isotope fractionation in solar system materials

Niel H. Williams [a], Manuela A. Fehr [b,c,*], Ian J. Parkinson [b,d], Maximilian B. Mandl [c], Maria Schönbächler [a,c]

[a] The University of Manchester, School of Earth, Atmospheric and Environmental Sciences, Manchester M139PL, UK
[b] The Open University, School of Environment, Earth and Ecosystem Sciences, Milton Keynes MK7 6AA, UK
[c] ETH Zürich, Institute of Geochemistry and Petrology, 8092 Zürich, Switzerland
[d] University of Bristol, School of Earth Sciences, Bristol BS8 1RJ, UK

ARTICLE INFO

Editor: Catherine Chauvel

Keywords:
Ti isotopes
Isotope fractionation
Chondrites
HED
Acapulcoites
NWA 7325

ABSTRACT

New methods to determine the titanium (Ti) mass-dependent isotope fractionation of solar system materials to high precision were developed by combining internally normalised Ti isotope data with double-spike analyses utilising a ^{47}Ti-^{49}Ti double spike. The procedure includes a three-stage ion-exchange separation procedure to isolate Ti from the sample matrix that provides high-purity Ti fractions that are necessary for high-precision Ti isotope analyses. Analyses of sample aliquots that were spiked before and after the ion-exchange separation procedure demonstrate that Ti isotope fractionation can be induced by the separation procedure. This outcome requires the addition of the double spike before the ion exchange separation procedure in order to accurately determine the natural mass-dependent Ti isotope fractionation of samples. Multiple double spike analyses of an Alfa Aesar Ti standard performed over eight months yielded a reproducibility (2σ standard deviation) of 0.033‰ for $\delta^{49/47}$Ti (differences in ^{49}Ti/^{47}Ti relative to the OL-Ti standard). Terrestrial sample analyses display a 2σ reproducibility of 0.018 to 0.031‰ for $\delta^{49/47}$Ti. Titanium isotope results for three terrestrial USGS magmatic reference samples (AGV-2, BHVO-2 and BCR-2) agree well with literature data and therefore demonstrate the accuracy and precision of the presented methodologies. Achondritic meteorites display an overall range of 0.75‰ for $\delta^{49/47}$Ti. The ungrouped achondrite NWA 7325 has a more positive composition by 0.64‰ for $\delta^{49/47}$Ti compared to all other investigated samples likely reflecting Ti isotope fractionation induced by magmatic differentiation associated with highly reducing conditions and potentially associated with oxide and plagioclase formation. In contrast, eucrites with $\delta^{49/47}$Ti of -0.020 ± 0.070 and -0.003 ± 0.033 and the first mass-dependent Ti isotope data for an acapulcoite (Dhofar 125; $\delta^{49/47}$Ti = 0.094 ± 0.033) show only limited magmatic Ti isotope fractionation. Chondrites also display a relatively restricted range of 0.085‰ for $\delta^{49/47}$Ti, including one calcium-aluminum rich inclusion (CAI) from Allende and the first mass-dependent Ti isotope data for two Rumuruti chondrites (NWA 753 and NWA 755). Furthermore, the mass-dependent Ti isotope composition of chondrites overlaps with that of eucrites and the acapulcoite Dhofar 125 indicating that nebular processes induce only limited Ti isotope fractionation. Additionally, the Ti isotope data indicate that thermal metamorphism also produced marginal Ti isotope fractionation at the bulk sample scale for chondrites. Small mass-dependent Ti isotope variations between different bulk meteorite samples are also evident, which might reflect sample heterogeneity. Importantly, the mass-dependent Ti isotope composition of the Earth and Moon overlap with the composition of the investigated chondrites, eucrites and acapulcoites within the 2 standard deviation uncertainties.

1. Introduction

Mass-dependent isotope fractionation of heavy elements is produced by biotic and abiotic processes and, hence, metal stable isotope systems have become powerful tools in both low and high-temperature geochemistry (e.g., Teng et al., 2017). In cosmochemistry, mass-dependent isotope fractionation of major and trace elements provide important constraints on processes in the solar nebula and planet formation (e.g., Georg et al., 2007). Titanium is a refractory lithophile element, which occurs abundantly (wt% concentrations) in most solar

* Corresponding author at: Department of Earth Sciences, ETH Zürich, 8092 Zürich, Switzerland.
E-mail address: manuela.fehr@erdw.ethz.ch (M.A. Fehr).

https://doi.org/10.1016/j.chemgeo.2020.120009
Received 3 July 2020; Received in revised form 16 October 2020; Accepted 25 November 2020
Available online 1 December 2020

system materials and is generally regarded as immobile during secondary alteration processes due to its high field strength (charge/radius ratio, Floyd and Winchester, 1978; Pearce and Norry, 1979). Hence, it is expected that most geochemical processes induce only little if any Ti isotope fractionation (Millet and Dauphas, 2014). However, Ti can be mobilised under certain pressure and temperature conditions (Ayers and Watson, 1991; Ayers and Watson, 1993). Experiments have furthermore demonstrated that evaporation can induce isotope fractionation of Ti (Zhang et al., 2014). Significant Ti isotope fractionation of up to 2.3‰ in $^{49}Ti/^{47}Ti$ is produced by magmatic differentiation in terrestrial igneous rocks (Deng et al., 2019; Deng et al., 2018a; Greber et al., 2017a; Hoare et al., 2020; Millet and Dauphas, 2014; Millet et al., 2016). Titanium isotope fractionation has also been documented for the achondritic aubrites, lunar samples (Greber et al., 2017b; Kommescher et al., 2020; Millet et al., 2016) and calcium-aluminum rich inclusions (CAIs) from carbonaceous chondrites (Davis et al., 2018; Niederer et al., 1985). In contrast, achondrites from the howardite-eucrite-diogenite (HED) group, angrites, martian meteorites and chondrites display only marginal to no Ti isotope fractionation compared to the terrestrial mantle composition (Deng et al., 2018b; Greber et al., 2017b).

Recent investigations of mass-dependent isotope fractionation utilising the double spike technique have revealed that it is a powerful method for the investigation of geological and biological processes (Arnold et al., 2010; Cameron et al., 2009; Gall et al., 2012; Ripperger and Rehkämper, 2007; Siebert et al., 2001). This methodology has also been applied in previous Ti isotope studies (e.g., Deng et al., 2018b; Greber et al., 2017b; Millet and Dauphas, 2014; Niederer et al., 1985). The presence of nucleosynthetic Ti isotope variations in meteorites (e.g., Leya et al., 2008; Trinquier et al., 2009) requires the combination of un-spiked and double-spiked analyses of meteorite samples to determine mass-dependent fractionation of Ti isotopes. This is in particular important for carbonaceous chondrites and achondrites, which have larger and more varied nucleosynthetic Ti isotope composition compared to the Earth than ordinary and enstatite chondrites. This approach has so far only been applied in combination with thermal ionisation mass spectrometic (TIMS) analyses (Niederer et al., 1985). Previous studies of meteorites that employed multi collector inductively coupled plasma mass spectrometry (MC-ICP-MS) and a doube spike technique have used literature data of un-spiked samples to correct Ti isotope fractionation data for mass-independent Ti isotope variations. This procedure is problematic due to sample heterogeneity in particular for investigations of chondrites that contain CAIs, which have large nucleosynthetic Ti isotope variations (Davis et al., 2018; Leya et al., 2009; Niederer et al., 1985). In this study, MC-ICP-MS that provides superior precision compared to TIMS is utilized to obtain high-precision Ti isotope analyses to investigate mass-dependent isotope fractionation of Ti in eleven chondritic and achondritic meteorite samples using a ^{47}Ti-^{49}Ti double spike. This study was part of the PhD thesis of N. Williams (Williams, 2014) and provides the first mass-dependent Ti isotope data for two Rumuruti like chondrites (R chondrites), an acapulcoite, and the unique ungrouped achondrite NWA 7325. Additionally, un-spiked aliquots of digested samples were also analysed by MC-ICP-MS to correct for mass-independent Ti isotope variations. The techniques presented here include an improved anion-exchange separation procedure for Ti, which represents a modified version based on Leya et al. (2007) and Schönbächler et al. (2004). The accuracy of the methodologies is verified through measurements of three terrestrial magmatic reference samples.

2. Samples

Bulk samples of two carbonaceous chondrites (Allende CV3 and Murchison CM2), two ordinary chondrites (Richardton H5 and Allegan H5), two R chondrites (Northwest Africa (NWA) 753 and NWA 755) and four achondrites (Pasamonte (eucrite, polymict breccia), Juvinas (eucrite, monomict breccia), Dhofar 125 (acapulcoite), NWA 7325 (ungrouped achondrite)) were measured for their Ti isotope composition. Also investigated was a CAI from Allende (CAI NV 1). In addition, three terrestrial USGS magmatic reference samples were included: BHVO-2 (Hawaiian basalt), BCR-2 (Columbia river basalt) and AGV-2 (andesite, Oregon).

3. Experimental

3.1. Sample preparation

Sample preparation was carried out in Class 10 work stations within a class 1000 clean room facility at the University of Manchester. Nitric acid and HCl were purified from AnalaR® grade reagents by triple sub-boiling distillation in quartz stills. Ultrapure grade HF (Romil), H_2O_2 (~30% vol. ultrapure grade) and H_2SO_4 (ultrapure grade) were purchased from Sigma Aldrich. 18.2 MΩ.cm grade H_2O from a Millipore® purification system was used throughout.

Meteorites were crushed in a boron carbide mortar under a laminar flow of filtered air. Samples were digested in Parr Bombs® following the procedures of Schönbächler et al. (2004). Terrestrial samples of up to 200 mg and meteorite samples of up to 100 mg were digested in 12 ml Savillex® vials containing 3 ml of concentrated HF and 1 ml of concentrated HNO_3. Sample vials were placed inside a 125 ml Parr Bomb and heated in an oven to 180 °C for 4.5 days. After digestion, the samples were dried down and re-dissolved in 5–10 ml of 6 M HCl.

Solutions were then split into two equal aliquots with terrestrial standard rocks and single element standards containing 50 μg Ti, whereas meteorite aliquots contained 9–35 μg Ti each. The first aliquot was directly processed through the three-stage ion-exchange chromatographic procedure described below to isolate Ti. The second aliquot was spiked prior to column chemistry with Ti double spike. Spiked sample aliquots were died down, redissolved using 1 ml 6 M HCl and refluxed twice to achieve spike-sample equilibration. Additionally, Ti fractions of samples that were prepared and analysed by Akram et al. (2013, 2015) for Zr isotopes were investigated for their Ti isotope composition. These samples were also measured both un-spiked and spiked, although the Ti double spike was added after the ion-exchange separation procedure. Titanium isotope results for samples that were spiked before and after the separation procedure were compared to investigate about possible fractionation due to the chemical separation technique.

A three-stage ion-exchange procedure (Table 1) was utilised to

Table 1
Titanium ion-exchange procedure[a].

Step	Volume	Acid
0.7 ml of Bio-Rad AG1-X8 resin, 200–400 mesh, chloride form[b]		
Resin cleaning[b]	14 ml	0.5 M HCl
	5 ml	6 M HCl - 1 M HF
	7 ml	H_2O
Column 1: removal of sample matrix		
Preconditioning	6 ml	4 M HF
Sample loading	5 ml	4 M HF
Matrix elution	5.5 ml	4 M HF
Ti and Zr	3 ml	6 M HCl - 1 M HF
Column 2: separation of Ti and Zr		
Preconditioning	7 ml	0.25 M H_2SO_4 + 1% H_2O_2
Sample loading and Ti	1 ml	0.25 M H_2SO_4 + 1% H_2O_2
Ti	8.5 ml	0.25 M H_2SO_4–1% H_2O_2
Zr	4 ml	6 M HCl - 1 M HF
Column 3: removal of remaining Ca, V, Cr and S		
Preconditioning	6 ml	4 M HF
Sample loading	1 ml	4 M HF
Matrix elution	5.5 ml	4 M HF
Matrix elution	5 ml	0.5 M HCl - 0.5 M HF
Ti	3 ml	6 M HCl - 1 M HF

[a] Modified after Schönbächler et al. (2004) and Leya et al. (2007).
[b] A fresh resin bed is prepared for each column stage.

separate Ti from the sample matrix based on methodologies detailed in Schönbächler et al. (2004) and Leya et al. (2007). Fluorinated ethylene propylene (FEP) columns filled with 0.7 ml Bio-Rad© AG1-X8 200–400 mesh anion exchange resin were used for all three stages of the separation procedure. The resin was cleaned with two column volumes (7 ml) of 0.5 M HCl followed by 5 ml of 6 M HCl −1 M HF before finally washing it with 1 column volume of H_2O for all three ion-exchange separation stages. The resin was conditioned with 6 ml of 4 M HF and samples were loaded utilising 5 ml of 4 M HF for the first separation step. If precipitate of CaF was observed, the samples were split prior to loading into two 1.5 ml centrifuge vials. The centrifuge vials were centrifuged for 20 min in order to separate the CaF precipitate prior to loading. This process was repeated three times such that a total volume of 5 ml of sample was produced. After the sample was loaded onto the column a further 0.5 ml of 4 M HF and 5 ml of 4 M HF were added to elute the majority of matrix elements. Titanium was eluted next in 3 ml of 6 M HCl - 1 M HF. The second ion-exchange separation step was employed to separate Ti from Zr. For this procedure the resin was preconditioned using 7 ml of 0.25 M H_2SO_4–1% H_2O_2, which was prepared on the same day in order to preserve the H_2O_2. The Ti was loaded using 1 ml of 0.25 M H_2SO_4–1% H_2O_2 and a further 0.5 ml of 0.25 M H_2SO_4–1% H_2O_2 was added. Titanium was eluted in the loading phase and an additional 8 ml of 0.25 M H_2SO_4–1% H_2O_2. The first column-stage of this procedure is repeated as an additional third column compared to Leya et al. (2007) to improve the separation of V, Ca and Cr from Ti and reduce the impact of these isobaric interfering elements onto the Ti isotope analyses. Samples were loaded in 1 ml 4 M HF for this final separation procedure, which also included an additional matrix elution step using 5 ml 0.5 M HCl - 0.5 M HF. The ion-exchange separation procedure of Schönbächler et al. (2004) was also employed by Akram et al. (2013, 2015) and the Ti fractions of that study were additionally processed using the described additional third ion-exchange separation step.

Full procedural blanks averaged 3 ng with a range of between 0.6 and 16 ng Ti. This is negligible compared to the 9–50 μg of Ti processed for samples and result in blank contributions of less than 0.2%.

Two in-house reference materials obtained from Alfa Aesar were utilized in this study, a Ti single element standard (Ti Alfa Aesar solution) and a Ti standard solution prepared from a Ti wire of 99.9985% purity (Ti Alfa Aesar wire). For the Ti Alfa Aesar wire standard, 68 mm of the Ti wire was cut off and then leached with 0.1 M HNO_3 for 5 min before being washed with H_2O and distilled ethanol. The wire was weighed and transferred to a Savillex® vial for digestion in 3 ml concentrated HF and 1 ml concentrated HNO_3.

3.2. Mass spectrometry and titanium double spike

3.2.1. Double spike preparation

Four of the five Ti isotopes (^{46}Ti to ^{50}Ti, Table 2) have to be selected for the double spike procedure. Previous studies utilized a ^{46}Ti-^{50}Ti (Niederer et al., 1985) or a ^{47}Ti-^{49}Ti double spike (Deng et al., 2018b; Kommescher et al., 2020; Millet and Dauphas, 2014). The use of ^{50}Ti in the double-spike procedure is not ideal, as nucleosynthetic Ti isotope anomalies in bulk meteorite samples are largest for ^{50}Ti (Leya et al., 2008; Trinquier et al., 2009) and ^{50}Ti has isobaric interferences from both Cr and V. The optimal double spike composition without the use of ^{50}Ti is a ^{47}Ti-^{49}Ti spike mixed in the proportion 50:50 based on error propagation simulations using the double spike toolbox by Rudge et al. (2009). Moreover, such a ^{47}Ti-^{49}Ti spike provides a robust range of double spike to sample mixtures over which the error propogation remains low (Millet and Dauphas, 2014; Rudge et al., 2009). Additionally, double spike compositions that provide near optimal intersection angles between the mass fractionation vectors of spiked and un-spiked samples (Galer, 1999) were also identified. This confirmed that a ^{47}Ti-^{49}Ti double spike mixed in the ratio of 47:53 is optimal based on own error propagation simulations (Williams, 2014). The optimal fraction of double spike in the sample-spike mixture was determined at 45% based on Rudge et al. (2009).

The Ti double spike was created as a mixture from two single spike solutions enriched in ^{47}Ti and ^{49}Ti. A total of 31 mg ^{47}Ti oxide (94.55% purity) and 29 mg ^{49}Ti oxide (96.25% purity) purchased from the Oak Ridge National Laboratory were separately dissolved for 3 days in 3 ml concentrated HF and 1 ml concentrated HNO_3 and subsequently diluted to a concentration of around 200 ppm. The two single spike solutions were mixed to obtain a final double spike solution with a total Ti concentration of ~34 ppm in 2 M HNO_3–0.2 M HF.

3.2.2. Mass spectrometric procedures

All isotopic sample measurements were performed using a Thermo Fisher Scientific Neptune MC-ICP-MS instrument at the Open University in Milton Keynes utilising an Aridus II desolvating sample introduction system, a normal sampler cone, and an X skimmer cone for analysis. Measurements were performed using a dynamic analysis routine to collect all five Ti isotopes and ^{44}Ca simultaneously in a first cycle and measure ^{50}Ti, ^{51}V and ^{53}Cr in a second cycle (Table 2). All masses beside ^{51}V were measured on the peak shoulder in either medium or high- mass resolution mode to resolve polyatomic interferences. This setup allows for interference corrections of Ca, V and Cr on Ti masses. Samples and standards were measured in 0.5 M HNO_3–0.005 M HF (for un-spiked analyses) or 0.5 M HNO_3–0.017 M HF (for analyses with Ti double spike). Data acquisition for samples and standards comprised collection of 40 ratios with 8.4 s integration for cycle 1 and 40 ratios with 4.2 s integration for cycle 2. On-peak background analyses were measured before every sample and standard analyses through collection of 20 ratios with integration of 8.4 s and 4.2 s respectively for cycles 1 and 2. A background correction was applied to sample and standard measurements by subtracting the average signal intensities of background measurements taken before and after the sample and standard measurements. Calcium interferences on ^{46}Ti and ^{48}Ti, as well as V and Cr interferences on ^{50}Ti were corrected using the measured ^{44}Ca, ^{51}V and ^{53}Cr data and included a mass bias correction. Each sample analysis was preceded and followed by a standard measurement. One sample measurement required 18 min and consumed ~800 μl sample solution. Average sensitivity for Ti was around 70 V/ppm in high mass resolution.

Table 2
Collector configuration for Ti isotopes and isobaric interferences.

	Cycle 1						Cycle 2		
Mass	44	46	47	48	49	50	50	51	53
Collector	L4	L1	C	H1	H2	H3	C	H1	H3
Isotope	^{44}Ca	^{46}Ti	^{47}Ti	^{48}Ti	^{49}Ti	^{50}Ti	^{50}Ti	^{51}V	^{53}Cr
Abundance (%)	2.08	8.25	7.44	73.72	5.41	5.18	5.18	99.75	9.50
Interferences									
Single charged		^{46}Ca		^{48}Ca		^{50}V, ^{50}Cr	^{50}V, ^{50}Cr		
Double charged atomic		^{92}Zr^{2+}	^{94}Zr^{2+}	^{96}Zr^{2+}					
Other interferences	$^{14}N_2^{16}O^+$ $^{28}Si^{16}O^+$	$^{30}Si^{16}O^+$	$^{28}Si^{19}F^+$		$^{14}N^{35}Cl^+$	$^{14}N^{36}Ar^+$	$^{14}N^{36}Ar^+$		$^{13}C^{40}Ar^+$

3.2.3. Unspiked mass-independent Ti isotope analyses

Titanium isotope measurements of un-spiked sample fractions (see supplementary table S1) and standard solutions were internally normalised relative to $^{49}Ti/^{47}Ti = 0.749766$ (Niederer et al., 1981) using the exponential law to correct for mass bias. Using internal normalization for mass bias correction, the two in-house reference materials (Ti Alfa Aesar solution and Ti Alfa Aesar wire) have identical Ti isotope compositions within uncertainties (Table 3).

3.2.4. Double spike calibration

To determine the Ti isotope composition of the double spike, two separate techniques were applied. All double spike calibrations and measurements were carried out relative to the gravimetrically prepared Ti Alfa Aesar wire standard. The isotopic analyses of the spike were externally normalised relative to Ca for mass bias correction of $^{50}Ti/^{47}Ti$. For the mass bias correction of $^{46}Ti/^{47}Ti$, $^{48}Ti/^{47}Ti$ and $^{49}Ti/^{47}Ti$ external normalization relative to Cr was utilised.

The $^{42}Ca/^{44}Ca$ and $^{53}Cr/^{52}Cr$ ratios that were used for this correction were optimized such that the mass bias correction procedure using Ca and Cr produced identical results for $^{46}Ti/^{47}Ti$, $^{48}Ti/^{47}Ti$ and $^{50}Ti/^{47}Ti$ as internal normalization to $^{49}Ti/^{47}Ti = 0.749766$ (Niederer et al., 1981). Finally, the optimised $^{42}Ca/^{44}Ca$ and $^{53}Cr/^{52}Cr$ ratios were utilised for the mass bias correction of the pure Ti double spike solution (Table 3).

The Ti concentration of the ^{47}Ti-^{49}Ti double spike was determined by reverse isotope dilution relative to the gravimetrically prepared Ti Alfa Aesar wire standard. This allows for Ti concentration determinations as a by-product of the mass-dependent Ti isotope analyses.

3.2.5. Double spike data reduction

The double spike data reduction was performed off line, using a geometric approach to solve the double spike equations in three-dimensional isotope space as described by Siebert et al. (2001). For the inversion process ^{46}Ti, ^{48}Ti and ^{49}Ti with ^{47}Ti as the denominator were utilised. The sample standard bracketing method was used to correct for small drifts within analytical sessions, in which the in-house Alfa Aesar wire standard was used as a bracketing standard. The mass-dependent Ti isotope data were calculated relative to the in-house Alfa Aesar wire standard:

$$\delta^{49/47}Ti_{Ti\ wire}\ (‰) = \left(\frac{{}^{49}Ti/{}^{47}Ti_{sample}}{{}^{49}Ti/{}^{47}Ti_{Alfa\ Aesar\ Ti\ wire\ standard}} - 1 \right) \times 10^3 \quad (1)$$

The Ti isotope results were then converted to a value relative to the Origins Laboratory Ti (OL-Ti) standard ($\delta^{49/47}Ti$ of Alfa Aesar Ti wire = 0.224 ± 0.017 relative to OL-Ti, as measured on a Neptune Plus MC-ICP-MS at ETH Zürich (Mandl, 2019), Table 4, Fig. 1) and reported as $\delta^{49/47}Ti$. Uncertainties displayed in the text, figures and tables are 2 standard deviations (2 SD) unless stated differently. In Table 4, 2 standard errors (2 SE = 2 SD / $\sqrt{n}$; n = number of analyses) are also reported. For terrestrial samples, 2 SD of multiple spiked sample analyses are reported. The 2 SD reproducibility of 0.033‰ of the Ti Alfa Aesar wire standard is given as 2 SD for solutions and samples that were measured less than 4 times and that had a 2 SD of <0.033‰.

For meteorite samples with mass-independent (nucleosynthetic) isotope variations, un-spiked mass-independent Ti isotope data (supplementary table S1) and double spike data are combined. For this, the measured Ti isotope ratios of the un-spiked meteorite samples is used in the double spike equations instead of the standard ratios. This combination was performed using individual un-spiked sample analyses, which were internally normalised and corrected for Ca interferences, and individual spiked sample measurements. Therefore, uncertainties of spiked and un-spiked measurements are included in the reported 2 SD and reflect multiple combinations of individual un-spiked and spiked sample analyses. The 2 SD reproducibility of 0.033‰ is given as 2 SD for samples that were measured less than 4 times and that had a 2 SD of <0.033‰.

4. Results

4.1. Titanium concentration data

Titanium concentration data of terrestrial reference and meteorite samples, as determined by isotope dilution using the presented methodologies, agree well with literature data (Table 4). The two studied R-chondrites (NWA 753 and NWA 755) and the acapulcoite Dhofar 125 have similar Ti contents to Antarctic R-chondrites (0.07–0.11 wt% TiO_2; Yanai et al., 1995) and other acapulcoite samples (0.07–0.13 wt% TiO_2; Palme et al., 1981; Yanai et al., 1995), respectively. The Ti content of the ungrouped meteorite NW 7325 is slightly lower at 0.04 wt% TiO_2 than that of the other analysed meteorites, whereas the Allende CAI (NV1) has a Ti content of 1.14 wt% TiO_2 typical for CAIs from CV3 carbonaceous chondrites (1–1.5 wt% TiO_2; MacPherson et al., 1988).

4.2. Mass-dependent Ti isotope data

The investigated samples display an overall spread of 0.75‰ in $\delta^{49/47}Ti$ (Table 4, Fig. 2). Most meteorite samples display a relative narrow range in $\delta^{49/47}Ti$ of −0.020 ± 0.070 to 0.094 ± 0.033, whereas the ungrouped achondrite NWA 7325 displays larger Ti isotope fractionation with a $\delta^{49/47}Ti$ of 0.733 ± 0.060. This study provides furthermore the first mass-dependent Ti isotope data for an acapulcoite with $\delta^{49/47}Ti = 0.094 \pm 0.033$ for Dhofar 125 and for two R chondrites that have $\delta^{49/47}Ti$ of 0.025 ± 0.045 (NWA 753) and $\delta^{49/47}Ti$ of 0.001 ± 0.033 (NWA 755). The Ti Alfa Aesar solution standard displays a more negative $\delta^{49/47}Ti$ compared to all investigated samples with −0.108 ± 0.033 (Table 4, Fig. 1).

4.3. Mass-dependent isotope fractionation during Ti separation

Mass-dependent Ti isotope data deduced for samples to which the Ti double spike was added after the ion-exchange separation procedure do not agree with results obtained for sample aliquots that were spiked before the separation procedure (Table 5, Fig. 3). Offsets between samples that were spiked before and after the separation procedure vary between −0.054 ± 0.033 and +0.194 ± 0.033‰ for $\delta^{49/47}Ti$. Therefore, samples that were spiked after the separation procedure are only used to assess Ti isotope fractionation due to laboratory chemical processing in Section 5.2 and are not included in Table 4 and Figs. 1, 2 and 5 that form the basis of the main discussion.

Table 3
Titanium isotopic compositions of Ti Alfa Aesar standards and the Ti double spike.

	$^{46}Ti/^{47}Ti$	2 SD	$^{48}Ti/^{47}Ti$	2 SD	$^{49}Ti/^{47}Ti$	2 SD	$^{50}Ti/^{47}Ti$	2 SD
Ti Alfa Aesar solution[a,b]	1.092971	0.000069	10.070618	0.000554	0.749766		0.729933	0.000050
Ti Alfa Aesar wire[b]	1.092994	0.000026	10.070272	0.000223	0.749766		0.729903	0.000042
^{47}Ti–^{49}Ti double spike[c]	0.006118	0.000004	0.078940	0.000031	1.057969	0.000050	0.008457	0.000003

[a] Longterm reproducibility.
[b] Internally normalised to $^{49}Ti/^{47}Ti = 0.749766$ (Niederer et al., 1981).
[c] Mass bias corrected externally relative to Cr ($^{46}Ti/^{47}Ti$, $^{48}Ti/^{47}Ti$ and $^{49}Ti/^{47}Ti$) and Ca ($^{50}Ti/^{47}Ti$)

Table 4
Titanium concentration and mass-dependent isotope fractionation data.

Samples	Description	TiO_2 (wt%)	TiO_2 (wt%)	n[a]	$\delta^{49/47}Ti_{\text{Ti wire}}$	$\delta^{49/47}Ti$	2 SD	2 SE
		This study	Literature					
Terrestrial reference samples								
BHVO-2 (aliq. 1)		2.75		3	−0.201	0.024	0.033[b]	
BHVO-2 (aliq. 2)		2.74		2	−0.184	0.040	0.033[b]	
Mean BHVO-2	Basalt, Hawaii	2.74	2.73[e]	5	−0.194	0.030	0.026	0.012
BCR-2 (aliq. 1)		2.27		4	−0.221	0.004	0.020	0.010
BCR-2 (aliq. 2)		2.25		2	−0.216	0.009	0.058	0.041
Mean BCR-2	Basalt, Columbia River	2.26	2.27[e]	6	−0.219	0.005	0.031	0.013
AGV-2	Andesite, Oregon	1.04	1.05[e]	5	−0.125	0.099	0.018	0.008
Ti Alfa Aesar solution				2	−0.333	−0.108	0.033[b]	
Ti Alfa Aesar wire				106	0.000		0.033	
OL-Ti				21	−0.224	0.000	0.017	
Meteorite samples								
Allende	CV3, USNM 3529	0.145	0.15 [f]	4	−0.138	0.086	0.045	0.023
Allende CAI NV 1	CAI CV3	1.14		3	−0.210	0.015	0.033[c]	
Murchison	CM2, USNM 5453	0.101	0.13[f]	3	−0.153	0.072	0.033[c]	
Allegan	H5	0.085	0.10[f]	3	−0.148	0.076	0.033[c]	
Richardton	H5	0.085	0.09[g]	4	−0.202	0.022	0.023	0.012
NWA 755	R-chondrite 3.7	0.096		3	−0.223	0.001	0.033[c]	
NWA 753	R-chondrite 3.9	0.093		3	−0.199	0.025	0.045	0.026
Juvinas	M[j]-eucrite, 40I(40G)	0.554	0.68 [h]	3	−0.244	−0.020	0.070	0.040
Pasamonte	P[j]-eucrite, USNM 897	0.661	0.65 [h]	3	−0.228	−0.003	0.033[c]	
Dhofar 125	Acapulcoite	0.097		3	−0.131	0.094	0.033[c]	
NWA 7325	Ungrouped achondrite	0.038	0.03[i]	3	0.509	0.733	0.060	0.035
Reproducibility of meteorites				35			0.033	
Reproducibility estimate of meteorites based on BCR-2				6			0.030[d]	

All Ti isotope data were measured relative to the Ti Alfa Aesar wire standard $\delta^{49/47}Ti_{\text{Ti wire}}$ and are reported relative to the OL-Ti standard ($\delta^{49/47}Ti$) for comparison to previous studies.
All samples were spiked before the Ti separation procedure.
$\delta^{49/47}Ti$, $\delta^{49/47}Ti_{\text{Ti wire}}$ and uncertainties for meteorites reflect the combination of unspiked and spiked analyses.
[a] Number of repeat analyses
[b] 2 SD reproducibility of 0.033 ‰ of Ti Alfa Aesar wire is given as 2 SD for <4 repeat analyses that had a 2 SD <0.033‰.
[c] 2 SD reproducibility of 0.033 ‰ of meteorites is given as 2 SD for <4 repeat analyses that had a 2 SD <0.033‰.
[d] 2 SD reproducibility based on combination of unspiked and spiked measurements.
[e] Jochum et al. (2016).
[f] Jarosewich (1990).
[g] Shima (1979).
[h] Duke (1967).
[i] Barrat et al. (2015).
[j] Monomict (M), polymict (P).

5. Discussion

5.1. Accuracy and reproducibility of mass-dependent Ti isotope data

5.1.1. Reproducibility of standard and sample analyses

Measurements of the Ti Alfa Aesar wire standard in 7 analytical sessions measured over a time-period of 8 months display a reproducibility (2 SD) of 0.033‰ in $\delta^{49/47}Ti$. A sample-standard bracketing procedure was applied to correct for small drifts over a single measurement session and a daily correction factor for small daily offsets in the absolute isotope ratios. The daily reproducibility (2 SD) of the Ti Alfa Aesar wire standard was on average 0.035‰ and varied from 0.024–0.046‰ for $\delta^{49/47}Ti$, also determined using the sample-standard bracketing procedure.

Terrestrial standard rocks that were measured over several analytical sessions display overall a similar reproducibility (2 SD) as the daily reproducibility of the standard at 0.018–0.031‰ for $\delta^{49/47}Ti$ and an average of 0.025‰ (Table 4). The reproducibility achieved for terrestrial samples is similar to those of Millet et al. (2014) and Deng et al. (2018b). Sample aliquots and the Ti Alfa Aesar solution standard that were only measured twice display a larger range in uncertainties and a 2 SD of up to 0.058‰ (Table 4, Fig. 1). Furthermore, individually processed sample aliquots of basalts display $\delta^{49/47}Ti$ values that overlap well within the stated uncertainties (Table 4, Fig. 1).

Meteorite analyses show an overall reproducibility of 0.033‰ (2 SD) for $\delta^{49/47}Ti$ reflecting the combined precision of un-spiked and spiked analyses (Table 4). The combination of unspiked and spiked terrestrial sample analyses of BCR-2 that were measured 6 times, respectively display a reproducibility of 0.030‰ (Table 4). This provides an additional uncertainty estimate for meteorites that were measured only 3–4 times and agrees well with the overall reproducibility of meteorite analyses (0.033‰).

5.1.2. Effect of spike to sample ratio

The Ti isotope composition of Ti double spike – Ti Alfa Aesar wire standard mixtures were analysed with variable spike/standard mixtures (proportion of DS in mixture (P) = 0.21–0.76; bracketing standard: P = 0.51–0.52) in order to investigate the robustness of the proportion of double spike used in the double spike standard mixture (Fig. 4b). The results demonstrate that the presented double spike methodology yields accurate mass-dependent Ti isotope data when the proportion of the double spike in the double spike – standard mixture is between 0.35 and 0.69. At higher proportions of double spike in the measured solutions, the accuracy of the $\delta^{49/47}Ti$ data deteriorate beyond the average daily reproducibility of the Ti Alfa Aesar wire standard. For standards that were significantly underspiked with a double spike proportion of 0.21 in the double spike – standard mixture, internal errors and the reproducibility of standards increase. The proportion of double spike in the samples varied from 0.34–0.71 and were measured relative to a ~ 1:1 mixture of spike to standard (P = 0.51). However, most sample aliquots had double spike proportions of 0.46–0.58. Samples that were slightly underspiked (P ~ 0.34) are the two R-chondrites and NWA 7325,

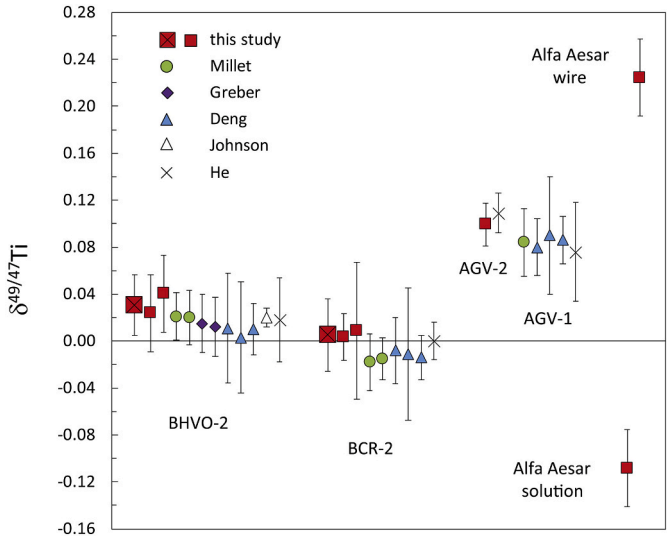

Fig. 1. Mass-dependent Ti isotope data of terrestrial reference samples and Ti standards reported relative to the OL-Ti standard. The $\delta^{49/47}$Ti data for BHVO-2 and BCR-2 from this study (large squares with cross) represent averages of two separately processed sample aliquots (smaller squares). Uncertainties are 2 SD for $\delta^{49/47}$Ti data from this study (Table 4) and literature data from Millet and Dauphas (2014), Millet et al. (2016): BHVO-2, BCR-2, Deng et al. (2018a,b) and He et al. (2020), whereas uncertainties for literature data from Millet et al. (2016: AGV-1), Greber et al. (2017a,b), Deng et al. (2019) and Johnson et al. (2019) represent 95% confidence intervals.

whereas Dhofar 125 was overspiked ($P = 0.71$). The effect of the spike to sample ratio is therefore considered negligible for the Ti mass-dependent isotope results of the samples investigated in this study.

5.1.3. Comparison to literature data

The two laboratory standards Ti Alfa Aesar solution ($\delta^{49/47}$Ti = −0.108 ± 0.033) and Ti Alfa Aesar wire ($\delta^{49/47}$Ti = 0.224 ± 0.033) measured in this study display significant Ti fractionation compared to the OL-Ti standard (Table 4, Fig. 1). The Ti Alfa Aesar solution standard yields the lowest $\delta^{49/47}$Ti value of any material determined here. Variations of up to 1.1‰ in $\delta^{49/47}$Ti have been documented for different Ti standards (Zhang et al., 2011), highlighting the need for a common reference standard to compare different mass-dependent Ti isotope fractionation studies. Previous studies of mass-dependent Ti isotope variations in chondrites (Deng et al., 2018b; Greber et al., 2017b) reported their data relative to different solution standards. To make an inter-laboratory comparison of their chondrite results with data presented here that were originally reported relative to the Ti Alfa Aesar wire standard (Williams, 2014), they used the difference of their results for USGS reference samples to correct for the standard offsets. Our cross-calibration of the Ti Alfa Aesar wire to the OL-Ti standard (Ti Alfa Aesar wire has a $\delta^{49/47}$Ti of 0.224 ± 0.017 relative to OL-Ti, Table 4, Fig. 1) allows a direct comparison of Ti isotope results for both reference and chondrite samples. By doing so, our Ti isotope data of two terrestrial USGS reference basalts agree well with those in the literature (Deng et al., 2019; Deng et al., 2018a; Deng et al., 2018b; Greber et al., 2017a; Greber et al., 2017b; He et al., 2020; Johnson et al., 2019; Millet and Dauphas, 2014; Millet et al., 2016) with $\delta^{49/47}$Ti = 0.030 ± 0.026 for BHVO-2 and $\delta^{49/47}$Ti = 0.005 ± 0.031 for BCR-2 (Fig. 1, Table 4). The USGS andesitic reference sample AGV-2 has a more positive Ti isotope composition with a $\delta^{49/47}$Ti of 0.099 ± 0.018 (Table 4, Fig. 1) compared to the two investigated basalts reflecting magmatic differentiation (Millet et al., 2016). Our Ti isotope data for AGV-2 overlaps within uncertainties with literature data of He et al. (2020). AGV-2 has within uncertainties an identical Ti isotope composition to AGV-1 determined by Millet et al. (2016), Deng et al. (2018a,b, 2019) and He et al. (2020). This further demonstrates the excellent agreement between the Ti isotope data obtained using the here presented methodologies and literature results.

The accuracy of the employed methodologies was further tested by processing an aliquot of double-spiked Ti standard through the column separation procedure described in this paper. The column-processed standard had an identical Ti isotope composition within uncertainties to the unprocessed standard with a $\delta^{49/47}$Ti of −0.019 ± 0.052 (2 SD, n = 2).

For three meteorite samples, literature $\delta^{49/47}$Ti data are also available. Our Ti isotope data for the CV chondrite Allende ($\delta^{49/47}$Ti = 0.086 ± 0.045) overlaps within uncertainties with the results from Greber et al. (2017b, $\delta^{49/47}$Ti = 0.052 ± 0.032, 95 % confidence intervals (c.i.)) and Deng et al. (2018b, $\delta^{49/47}$Ti = 0.112 ± 0.089, 2 SD (recalculated from 2 SE)) (Fig. 2). Results for the CM chondrite Murchison ($\delta^{49/47}$Ti = 0.072 ± 0.033) and the eucrite Juvinas ($\delta^{49/47}$Ti = −0.020 ± 0.070) from our study also agrees with literature data of Deng et al. (2018b, $\delta^{49/47}$Ti = 0.037 ± 0.042) and Greber et al. (2017b, $\delta^{49/47}$Ti = -0.025 ± 0.030, 95% c.i.), respectively (Fig. 2).

The comparison of the Ti isotope data for terrestrial reference samples and meteorites therefore provides evidence for the accuracy of the presented methodologies. Furthermore, the anion-exchange separation procedure we utilize provides the opportunity for the combined study of Zr and Ti isotopes (Leya et al., 2008; Leya et al., 2007; Schönbächler et al., 2004) and avoids usage of solvent-based resins such as the TODGA (DGA) resin that was employed by Greber et al. (2017b) and Deng et al. (2018b). Organics derived from solvent-based resins can affect mass-bias and thereby produce analytical artifacts, as was documented for e.g., the TRU- (Gault-Ringold and Stirling, 2012; Murphy et al., 2016) and Ln-spec resins (e.g., Saji et al., 2016) for the Cd and Nd isotope systems. Oxidising agents ($HNO_3 \pm H_2O_2$) were utilised by Greber et al., 2017b and Deng et al., 2018b to treat the final Ti fractions and therefore minimise the effect of remaining organics from the TODGA (DGA) resin. The available data suggest that such effects of remaining organics are insignificant for Ti within the presented uncertainties, given the agreement between the Ti isotope data of this study and literature (Fig. 2).

5.1.4. Nucleosynthetic Ti isotope variations

Previous mass-dependent Ti isotope studies used mass-independent Ti data from the literature to correct for nucleosynthetic effects of meteorite samples (Greber et al., 2017b; Deng et al., 2018b), whereas here unspiked Ti data are combined with double-spike Ti analyses obtained on the same sample dissolution to derive the $\delta^{49/47}$Ti values for meteorites (Table 4). Our unspiked Ti isotope data (supplementary table S1) generally fall in the range of reported literature data (Leya et al., 2008; Trinquier et al., 2009; Zhang et al., 2012; Burkhardt et al., 2017). Utilizing average mass-independent Ti data from the literature for different meteorite classes (as applied by Greber et al., 2017b) instead of the average measured unspiked Ti isotope data (supplementary table S1) for this correction would result in slight differences in the obtained $\delta^{49/47}$Ti data. Estimated shifts are insignificant at <0.01‰ for the ordinary chondrites Richardton ($\delta^{49/47}$Ti = 0.022 ± 0.023) and Allegan ($\delta^{49/47}$Ti = 0.076 ± 0.033) confirming their slightly different mass-dependent Ti isotope composition (Table 4), whereas their unspiked mass-independent Ti isotope composition is nearly identical and close to average literature data. However, the difference between using literature data and data obtained on the same sample dissolution is most prominent for Juvinas with a resulting difference of ~0.038‰. Thus, using literature data would shift the composition of Juvinas to ~0.018, which is close to that of Pasamonte ($\delta^{49/47}$Ti = −0.003 ± 0.033, Table 4). This estimated shift, however, is not directly comparable to our reported data. To obtain a more realistic estimate of $\delta^{49/47}$Ti and its associated errors, we randomly combined individual unspiked and spiked analyses of a sample to calculate the $\delta^{49/47}$Ti data (Table 4).

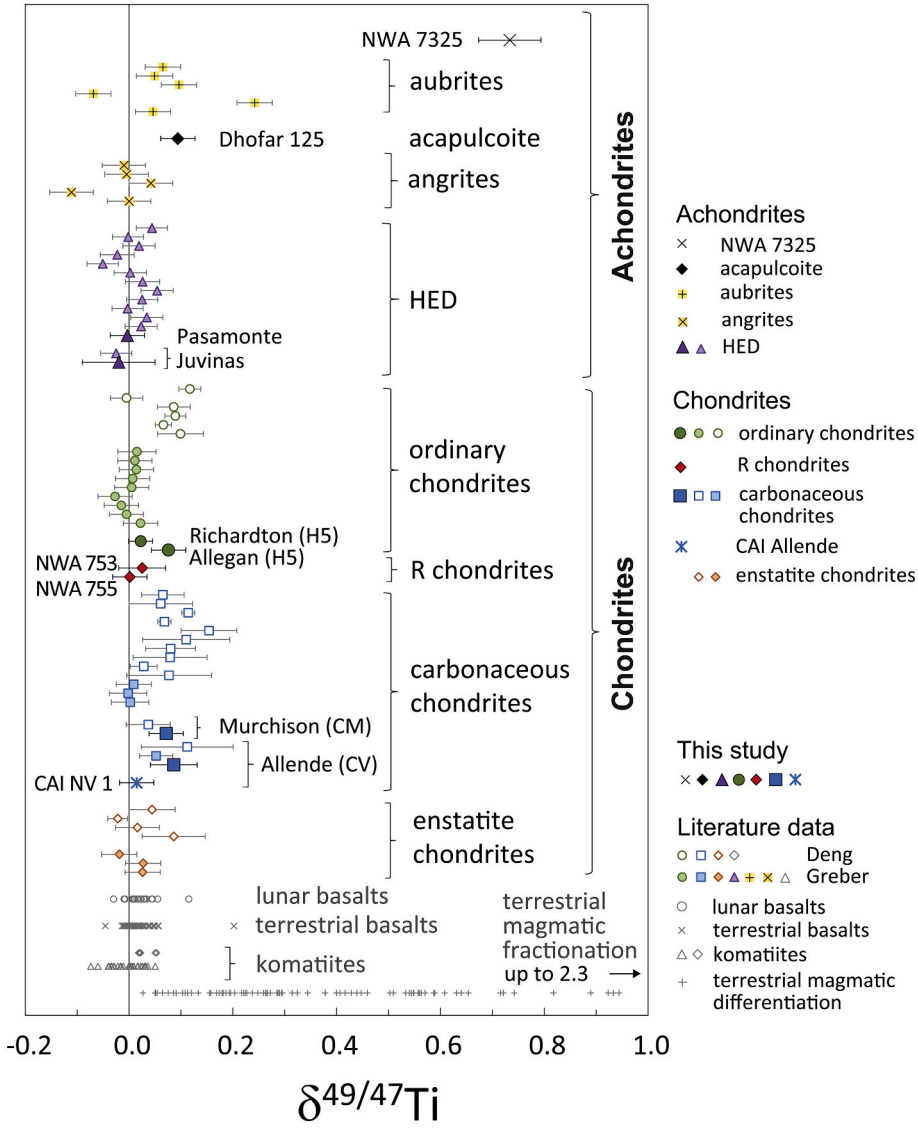

Fig. 2. Mass-dependent Ti isotope data of meteorites. Literature data for meteorites, lunar basalts, terrestrial basalts, komatiites and magmatic differentiation sequences are from Millet and Dauphas (2014), Millet et al. (2016), Greber et al. (2017a,b), Deng et al. (2018a,b, 2019), Kommescher et al. (2020) and Hoare et al. (2020). The $\delta^{49/47}$Ti data are reported relative to the OL-Ti standard. Displayed uncertainties are 2 SD for data from this study (Table 4) and Deng et al. (2018b) and 95% confidence intervals for data from Greber et al. (2017b).

Table 5
Titanium isotope fractionation of separation procedure.

Samples	$\delta^{49/47}$Ti $_{offset}$	2 SD	2 SE
BHVO-2	0.026	0.033[a]	
BCR-2	−0.022	0.036	0.025
AGV-2	0.048	0.033[a]	
Murchison	−0.054	0.033[b]	
Allende aliquot 1	0.073	0.048	0.028
Allende aliquot 2	0.128	0.033[b]	
Allegan	−0.017	0.033[b]	
Richardton	0.194	0.033[b]	
Pasamonte	−0.003	0.059	0.034

Ti isotope results of sample aliquots that were spiked after the separation procedure. Data are reported relative to results reported in Table 4 for sample aliquots that were spiked before the separation procedure.

[a] 2 SD reproducibility of 0.033 ‰ of Ti Alfa Aesar wire is given as 2 SD for <4 repeat analyses that had a 2 SD <0.033 ‰.

[b] 2 SD reproducibility of 0.033 ‰ of meteorites is given as 2 SD for <4 repeat analyses that had a 2 SD <0.033 ‰.

5.2. *Titanium isotope fractionation due to laboratory chemical processing*

Samples to which the Ti double spike was added after the chemical separation procedure display variable offsets in their Ti isotope fractionation compared to samples that were spiked before the separation procedure at −0.054 ± 0.033 to +0.194 ± 0.033‰ for $\delta^{49/47}$Ti with an average of 0.043 ± 0.165‰ (Table 5, Fig. 3). This provides evidence of Ti isotope fractionation induced by the separation procedure. Samples are dissolved in 4 M HF for the first column step (Table 1) and are centrifuged before sample loading to remove fluoride precipitates. He et al. (2020) reported Ti isotope fractionation for samples that were dissolved in 2 M HF as a consequence of formation of fluoride precipitates, resulting in sample solutions with heavier Ti isotope composition than the precipitates. Several of the here studied sample aliquots that were spiked after the column procedure also have a heavier Ti isotope composition compared to samples that were spiked before the separation procedure. Therefore, Ti isotope fractionation due to the formation of fluoride precipitates likely caused part of the observed discrepancies between $\delta^{49/47}$Ti results for sample aliquots that were spiked before and after the separation procedure (Table 5, Fig. 3). Furthermore, ion-exchange separations can induce isotope fractionation if column yields are incomplete (e.g., Anbar et al., 2000; Schönbächler et al., 2007). Therefore, the applied anion-exchange column procedure

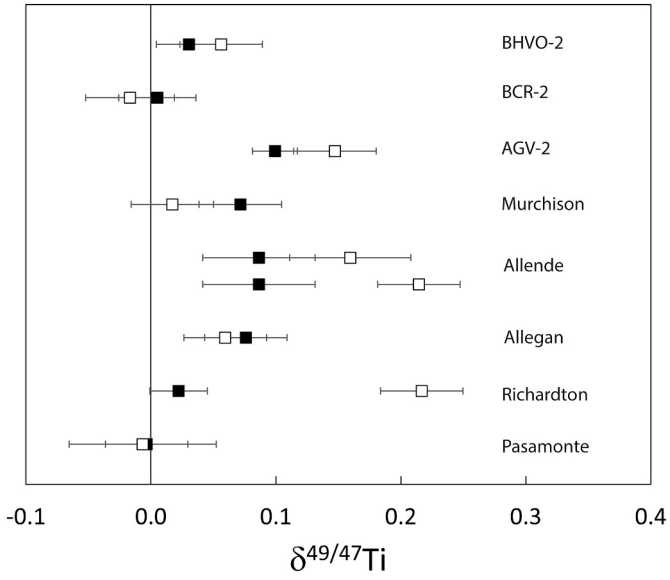

Fig. 3. Mass-dependent Ti isotope data of sample aliquots that were spiked before (filled symbols) and after (open symbols) the column separation procedure. Uncertainties are 2 SD.

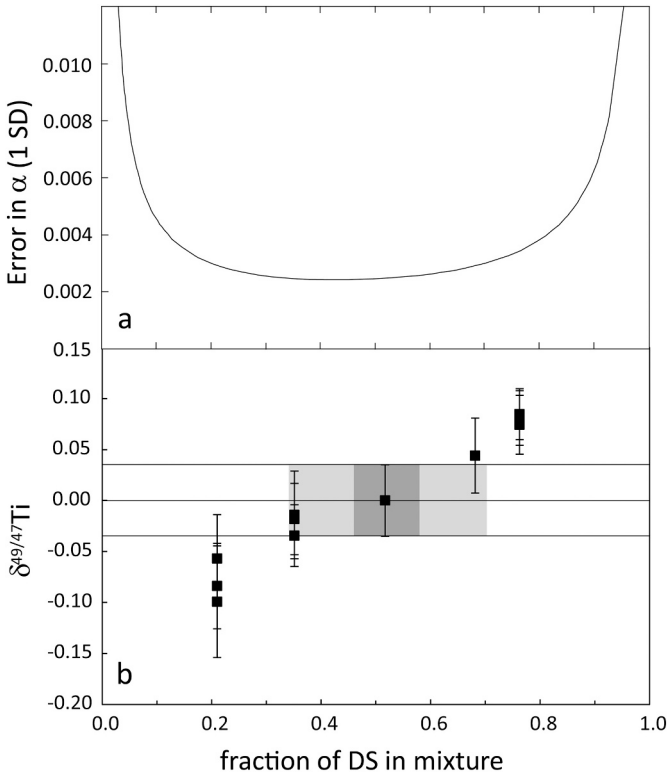

Fig. 4. (a) Expected uncertainties on the fractionation factor (α) after double spike calculations are given as a function of the ratio of double spike in the double spike (DS) - sample mix for different DS mixtures. Results were obtained by the error minimization code of Rudge et al. (2009). (b) Titanium isotope data for various mixtures of DS and Ti Alfa Aesar wire standard. The results are reported relative to data acquired at proportion of double spike to standard of approximately 1:1 (DS proportion of 0.52 in mixture). The light grey rectangle denotes the range of mixtures present for sample analyses. Dark grey rectangle: all except 4 samples. Displayed uncertainties for under- and overspiked mixtures denote the internal precision (2 SE) of the analyses. The error band displays the average daily reproducibility (2 SD) of Ti Alfa Aesar wire standard analyses with DS proportions of ~0.5 in the mixture.

may also have contributed to the observed variations and could provide an explanation for fractionation towards a heavier and lighter isotope composition. However, four of the investigated nine sample aliquots displayed no evidence of mass-dependent Ti isotope fractionation by the chemical separation procedure given the average reproducibility of 0.025 and 0.033‰ for terrestrial and meteorite sample data. The amount of fractionation induced by the separation procedure varies and therefore only mass-dependent Ti isotope fractionation data of samples spiked before the ion-exchange technique yield accurate $\delta^{49/47}$Ti isotope data. Since other Ti separation methods (Deng et al., 2018b; Millet and Dauphas, 2014; Zhang et al., 2011) use part of the method presented here (first and third column, originally from Schönbächler et al., 2004), this also applies for those separation procedures.

5.3. Mass-dependent titanium isotope fractionation in meteorites

5.3.1. Titanium isotope fractionation of chondrites

The chondrites investigated here display limited Ti isotope fractionation (Table 4) with a range of 0.001 ± 0.033 to 0.086 ± 0.045 for $\delta^{49/47}$Ti that overlaps with literature data (Deng et al., 2018b; Greber et al., 2017b, Fig. 2). The Ti isotope value for CAI NV 1 from Allende (Table 4) is also in line with previous data (Davis et al., 2018; Niederer et al., 1985) and displays limited fractionation with a $\delta^{49/47}$Ti of 0.015 ± 0.033 that is only 0.071‰ lower than bulk Allende. Chondrites are an assemblage of material from the solar nebula and include not only fine-grained matrix, but also chondrules and CAIs that formed in the nebula. In this environment, mass-dependent isotope fractionation can be generated through evaporation and condensation processes. The limited Ti isotope fractionation observed in chondrites is expected for equilibrium processes because this type of mass-dependent isotope fractionation is predicted to be small at high temperatures (e.g., Schauble, 2004) and Ti is a refractory element with a high half mass condensation temperature of 1565 K (Wood et al., 2019). The Ti isotope data (Fig. 2) is in agreement with mass-dependent data from other refractory elements. These elements generally display limited isotope fractionation in bulk chondrites (around 0.2‰/amu or less for Mo, Ru, Pd, REE, W and Pt (Albalat et al., 2012; Breton and Quitte, 2014; Burkhardt et al., 2014; Creech et al., 2017a,b; Hopp and Kleine, 2018; Krabbe et al., 2017; McCoy-West et al., 2017)). This suggests that near equilibrium processes dominated in the solar nebula and kinetic isotope fractionation was suppressed by high dust/gas ratios (e.g., Alexander et al., 2008).

Experimental data, however, demonstrated that substantial kinetic Ti isotope fractionation can be produced by evaporation (Zhang et al., 2014). Large variations of up to 38‰ were documented for hibonite grains in FUN (fractionated and unidentified nuclear effects) inclusions (Ireland et al., 1992) and up to 8‰ for bulk values of normal and FUN CAIs (Davis et al., 2018; Niederer et al., 1985). The average mass-dependent Ti isotope composition of CAIs, however, is close to that of terrestrial basalts (Davis et al., 2018) and this suggests that CAIs do not strongly influence the bulk chondrite compositions. This stands in contrast to nucleosynthetic Ti isotope variations carried by CAIs. They can range up to 1‰ for ^{50}Ti and affect the isotopic bulk rock compositions (e.g., Davis et al., 2018; Leya et al., 2009; Niederer et al., 1985; Trinquier et al., 2009).

While refractory elements in general show very limited isotope fractionation in chondrites, they exhibit significant mass-dependent Ca isotope variations of up to 0.25‰/amu (Amsellem et al., 2017; Huang and Jacobsen, 2017; Simon and DePaolo, 2010; Valdes et al., 2014). Calcium has a similar half mass condensation temperature (1535 K, Wood et al., 2019) to Ti (1565 K) and therefore should behave similarly to Ti. The difference between Ti and Ca isotopes in chondrites is likely related to CAIs (see discussion in Deng et al., 2018b; Greber et al., 2017b). While CAIs show an average $\delta^{49/47}$Ti value close to that of terrestrial basalts (Davis et al., 2018), their average Ca isotope composition is shifted towards lighter composition (Huang et al., 2012; Niederer and Papanastassiou, 1984) and offset, by mass balance, the bulk

chondrite composition towards lighter values.

5.3.1.1. A bimodal distribution. The R chondrites are highly oxidised and form a distinct chondrite group (Bischoff et al., 2011). The two R chondrites NWA 753 ($\delta^{49/47}$Ti = 0.025 ± 0.045) and NWA 755 ($\delta^{49/47}$Ti = 0.001 ± 0.033) have Ti isotope compositions very close to the ordinary chondrite Richardton (H5) ($\delta^{49/47}$Ti = 0.022 ± 0.023, Table 4). The Ti isotope data for the H5 chondrite Allegan and the two carbonaceous chondrites Allende and Murchison overlap with the composition of the R chondrites and Richardton (H5). They, however, consistently tend towards slightly heavier $\delta^{49/47}$Ti values from 0.072 ± 0.033 to 0.086 ± 0.045 (Fig. 2, Table 4). Hence, the Ti isotope data of chondrites appear to form a bimodal distribution (Fig. 2). This is also reflected in the literature data, although this data display a relatively large spread with −0.027 ± 0.033 to 0.154 ± 0.024 for $\delta^{49/47}$Ti (Fig. 2, Deng et al., 2018b; Greber et al., 2017b), mainly defined by the data of Deng et al. (2018b). While the Ti isotope variations appear unrelated to chondrite groups (Fig. 2) and metamorphic grade (Fig. 5), there are indications for potential systematic differences between the different data sets (Fig. 2). The average $\delta^{49/47}$Ti value of chondrites from Greber et al. (2017b) is slightly lower with 0.007 ± 0.039 (2 SD) compared to the data of Deng et al. (2018b) with 0.071 ± 0.084. The average of the 6 chondrites presented in this study is intermediate with $\delta^{49/47}$Ti of 0.047 ± 0.070. The majority of the Ti isotope data for different bulk chondrites (Fig. 2) are not, or only barely, resolvable if conservative uncertainty estimates (2 standard deviations) are applied, which makes it difficult to exclude analytical artifacts. However, the Ti isotope data for terrestrial reference rocks and the carbonaceous chondrites Allende and Murchison of the different studies agree within uncertainties (Figs. 1 and 2, Deng et al., 2018b; Greber et al., 2017b). This would argue against analytical artifacts and for Ti isotope variations inherent to the sample. In the following potential implications are discussed.

5.3.1.2. Sample heterogeneity and nucleosynthetic Ti isotope variations. It is well documented that chondrites and their components (CAIs, chondrules and matrix) carry significant mass-independent, nucleosynthetic Ti isotope variations (Davis et al., 2018; Gerber et al., 2017; Leya et al., 2009; Niederer et al., 1985; Trinquier et al., 2009) that stem from the heterogeneous distribution of presolar grains in the solar nebula (e.g., Ek et al., 2020). These grains formed in different stellar environment before the birth of our sun and carry the extreme isotopic composition of their stellar formation sites (e.g., Zinner, 2014). The actual nucleosynthetic Ti isotope composition of the measured bulk aliquot is a crucial parameter of the double spike calculations. For this reason, mass-dependent and mass-independent data was obtained from the same sample aliquot in this study. Previous work used literature data and therefore sample heterogeneity in the nucleosynthetic Ti isotope composition, propagated through the double spike inversion, could have induced at least part of the observed Ti isotope variations. For example, Deng et al. (2018b) reported variable $\delta^{49/47}$Ti results of up to 0.1‰ for different sample digestions of carbonaceous chondrites. These chondrites display distinct nucleosynthetic Ti isotope compositions for major components (chondrules, matrix and CAIs; Davis et al., 2018; Gerber et al., 2017; Leya et al., 2009; Niederer et al., 1985; Trinquier et al., 2009). A non-representative sampling of these components likely lead to the nucleosynthetic Ti isotope heterogeneity for bulk rock aliquots reported for, e.g., the CV chondrite Allende (Burkhardt et al., 2017; Leya et al., 2008; Trinquier et al., 2009; Zhang et al., 2011; Zhang et al., 2012). An unrepresentative sampling of chondrite components may also be reflected in the Ti content of bulk meteorite samples, although presolar gains do not substantially contribute to the bulk Ti content, but chondrules and CAIs may do so. The ordinary (Allegan and Richardton: 0.085 wt% TiO_2) and R-chondrites (NWA 755 and NWA 753: 0.096 and 0.093 wt% TiO_2) are considered to be representative bulk samples based on their nearly identical Ti contents (Table 4). Allegan and Richardton furthermore have a slightly distinct mass-dependent Ti isotope composition (Fig. 2), while having identical Ti contents (Table 4). Murchison has a slightly lower Ti content at 0.1 wt% TiO_2 compared to literature data (0.13 wt% TiO_2; Jarosewich, 1990), indicating it might be slightly enriched in matrix that has a lower Ti content compared to chondrules and CAIs (Table 4, MacPherson et al., 1988; Gerber et al., 2017). The effect of an incorrect nucleosynthetic Ti isotope composition in the double-spike calculations is to some extent mitigated by avoiding ^{50}Ti that generally carries the largest nucleosynthetic offsets. This has been applied for all recent double spike studies (Deng et al., 2018b; Greber et al., 2017b; Millet et al., 2016). Beside ^{50}Ti, the next largest nucleosynthetic offsets exist for ^{46}Ti and they are most expressed in carbonaceous chondrites. For Allende, ε^{46}Ti data range from 0.53 to 0.94 (Burkhardt et al., 2017; Trinquier et al., 2009; Zhang et al., 2012), which would translate into corrections of 0.06 to 0.1‰ and therefore a difference of ~0.04‰ in $\delta^{49/47}$Ti depending on the choice of un-spiked sample data. This is likely close to the maximum expected shift because nucleosynthetic Ti isotope variations of bulk samples from other meteorite classes are generally smaller (see e.g. Haack et al., 2019 for ordinary chondrites), as are nucleosynthetic shifts in ε^{48}Ti that also need correction. Nevertheless, since the analytical precision of $\delta^{49/47}$Ti is smaller than the maximum

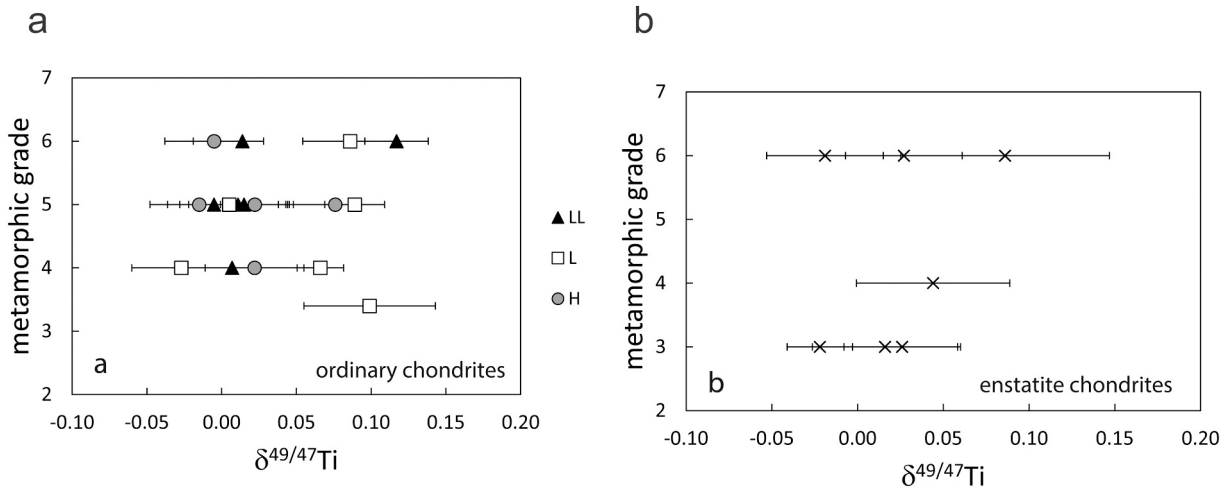

Fig. 5. Mass-dependent Ti isotope data for ordinary and enstatite chondrites (from Table 4 and Greber et al. (2017b) and Deng et al., 2018b) versus metamorphic grade. Displayed uncertainties are 2 SD (Table 4, this study and Deng et al., 2018b) and 95% confidence intervals for data from Greber et al. (2017b), $\delta^{49/47}$Ti data are reported relative to the OL-Ti standard.

offsets, they are significant. They are further relevant because only small sample amounts are necessary for a high-precision Ti isotope analysis by MC-ICP-MS, generally as little as ≤1 μg Ti (~1–2 mg bulk chondrite). In the present study, sample powders of ≥100 mg were digested, whereas previous works used very small aliquots for mass-dependent Ti isotope analyses (Deng et al., 2018b: 6–25 mg; Greber et al., 2017b: 50–100 mg, personal communication). In addition, the literature data used in these studies for the correction obtained their nucleosynthetic compositions on small sample aliquots (Zhang et al., 2012: 1–10 mg; Trinquier et al., 2009: 10–100 mg).

Therefore, it is possible that sample heterogeneity is responsible for at least part of the observed $\delta^{49/47}$Ti variations in the literature (Deng et al., 2018b; Greber et al., 2017b). In the present study, the effect of such heterogeneities is minimised because un-spiked and spiked Ti isotope data are obtained from the same sample aliquots.

5.3.1.3. Mass-dependent Ti isotope variations & thermal metamorphism. Small scale sample heterogeneity in $\delta^{49/47}$Ti potentially also affected the data. This is because CAIs exhibit relatively large $\delta^{49/47}$Ti variations (Davis et al., 2018) and small sample aliquots may contain different amounts of CAIs. This effect is mainly relevant for carbonaceous chondrite (CV, CM, CO) data because of their higher CAI abundances (Hezel et al., 2008), while ordinary chondrites have low CAI contributions. Instead, most ordinary chondrites experienced thermal metamorphism. They exhibit sharp increases in Ti^{4+} relative to Ti^{3+} between type 3.5 and type 4 samples in both olivine and pyroxene due to metamorphism (Simon et al., 2016). Large fractionation associated with redox processes is known for many isotopic systems and are also expected for Ti based on first principles calculations (Wang et al., 2020). Therefore, it is possible that distinct $\delta^{49/47}$Ti values develop in different phases of ordinary chondrites during metamorphism and this would require larger sample aliquots to be analysed for the data to be representative for bulk rock. Moreover, the effect of sample heterogeneity may vary with increasing grade of metamorphism due to new mineral phases that form including Ti rich chromite, which can be up to 0.2 mm in size (Huss et al., 2006). So far, only bulk rock mass-dependent Ti isotope data are available for ordinary chondrites. Generally, they show no trend with sup-groups (*H*, *L*, LL) or metamorphic grade (Fig. 5). Titanium isotope fractionation is larger for two LL6 chondrites compared to the available data for LL5 and LL4 chondrites (Fig. 5). However, this is a very limited data set. It is noteworthy that the two H5 chondrites Allegan and Richardton (Table 4) display distinct isotopic compositions. This indicates that indeed Ti isotope fractionation occurs during thermal metamorphism in ordinary chondrites and that mass-dependent Ti isotope data could be used to further constrain the metamorphic evolution on the ordinary chondrite parent bodies.

5.3.1.4. Chondritic Earth. Compositional differences in the early solar system are evident based on mass-dependent variations between different chondrite groups and/or a non-chondritic silicate Earth composition for the major elements Mg, Si, Ca, Ni (potentially also Fe) (e.g., Amsellem et al., 2017; Dauphas et al., 2017; Hin et al., 2017; Huang and Jacobsen, 2017; Klaver et al., 2020; Zambardi et al., 2013). They are generally considered to be related to volatility (evaporation and condensation processes, e.g., for Ca) and/or core formation. The mass-dependent Ti isotope composition of chondrites (Deng et al., 2018b; Greber et al., 2017b) overlaps with that of terrestrial basalts, komatiites and lunar basalts ($\delta^{49/47}$Ti of −0.074 ± 0.030 to 0.200 ± 0.030 and most data fall in the range of −0.039 to 0.056 for $\delta^{49/47}$Ti, Deng et al., 2019; Deng et al., 2018a; Greber et al., 2017a; Greber et al., 2017b; Hoare et al., 2020; Kommescher et al., 2020; Mandl, 2019; Millet et al., 2016, Fig. 2). Therefore, the available Ti isotope data support a chondritic Earth in terms of Ti isotope fractionation. However, several chondrites, including the two carbonaceous chondrites, have slightly heavier compositions compared to terrestrial basalts and komatiites (Fig. 2). Consequently, additional $\delta^{49/47}$Ti data for representative samples of the silicate Earth and chondrites will be necessary to further evaluate whether the Earth is chondritic in its mass-dependent Ti isotope composition.

5.3.2. Titanium isotope fractionation of achondrites

Achondrites show evidence of significant mass-dependent Ti isotope fractionation with $\delta^{49/47}$Ti variations in the range of 0.75 (Table 4, Fig. 2) and therefore display larger Ti isotope fractionation than chondrites. The ungrouped achondrite NWA 7325 possess the heaviest $\delta^{49/47}$Ti value of all investigated meteorites and hence, the significance of this result will be discussed in Section 5.3.2.1. With the exception of NWA 7325, the three investigated achondrites display a relatively narrow range of −0.020 ± 0.070 to 0.094 ± 0.033 for $\delta^{49/47}$Ti overlapping with the composition of chondrites, terrestrial and lunar basalts and terrestrial komatiites (Table 4, Fig. 2). The data for the two basaltic eucrites Juvinas ($\delta^{49/47}$Ti = −0.020 ± 0.070) and Pasamonte ($\delta^{49/47}$Ti = −0.003 ± 0.033) agree within uncertainties with results from Greber et al. (2017b) for eucrites and diogenites. These meteorites belong to the HED clan that is thought to originate from the asteroid Vesta (Binzel and Xu, 1993). Our results further support the results of Greber et al. (2017b). These authors concluded that Ti isotope fractionation in mafic systems such as that of the HED meteorites is limited because (i) Ti does not exist in different oxidation states (Ti^{3+} versus Ti^{4+}) and (ii) no Fe-Ti oxide (e.g., ilmenite) has reached saturation. Fractional crystallisation and removal of Fe-Ti oxides with a light Ti isotope composition has been favoured to explain the positive correlation of $\delta^{49/47}$Ti with SiO_2 concentration in more evolved terrestrial magmatic rocks (Deng et al., 2019; Deng et al., 2018a; Greber et al., 2017a; Hoare et al., 2020; Millet and Dauphas, 2014; Millet et al., 2016).

The acapulcoite Dhofar 125 displays a slightly higher $\delta^{49/47}$Ti of 0.094 ± 0.033 than Juvinas and Pasamonte ($\delta^{49/47}$Ti = −0.020 ± 0.070 and 0.003 ± 0.033, Table 4) and literature data of HED meteorites and angrites (Fig. 2). Acapulcoites, including Dhofar 125, are residues that experienced low degrees of partial melting (1–4 vol%) (e.g., Keil and McCoy, 2018; Mittlefehldt et al., 1998; Patzer et al., 2004). Partial melting of the Earth's mantle produces very limited Ti isotope fractionation, as indicated by Ti isotope data of mid-ocean ridge and island basalts, komatiites and a small number of peridotites (Deng et al., 2018a; Greber et al., 2017b; Millet et al., 2016). By contrast, the achondritic aubrites, which are also residue of partial melting, display larger fractionation ($\delta^{49/47}$Ti = −0.069 ± 0.034 to 0.242 ± 0.034, Fig. 2, Greber et al., 2017b). This is likely related to the more reducing conditions on the aubrite parent body. This environment allowed for the formation of Ti rich-sulfides, which likely favour Ti^{3+} in contrast to the prevalent Ti^{4+} in silicates. The extraction of Ti by a sulphide melt during core formation may explain the heavier composition of aubrites (Greber et al., 2017b; Wang et al., 2020). However, acapulcoites are less reduced than aubrites (Righter et al., 2016) and Ti has not been detected in sulphide (Patzer et al., 2004). This implies that sulfide melt extraction from the acapulcoites cannot explain the slightly heavier Ti isotope data of Dhofar 125 compared to HED meteorites and basalts from terrestrial magmatic systems.

Acapulcoites, however, contain Ti bearing oxide minerals such as chromite (Hutchison, 2004), which might have a fractionated Ti isotope composition. Therefore, sample heterogeneity could be the cause of the slightly heavier Ti isotope composition for Dhofar 125. In any case, Dhofar 125 only experienced limited fractionation and its $\delta^{49/47}$Ti value (0.094 ± 0.033) falls within the range of compositions defined by bulk chondrites. Further investigations would help to reveal whether the Ti isotope composition of Dhofar 125 is characteristic for acapulcoites. In summary, magmatic processes induced very limited mass-dependent Ti isotope variations in acapulcoite and the HED meteorites in contrast to NWA 7325, aubrites and terrestrial evolved igneous rocks (Fig. 2; Deng et al., 2019; Greber et al., 2017a; Greber et al., 2017b; Millet et al., 2016).

5.3.2.1. Titanium isotope fractionation of the achondrite NWA 7325. The ungrouped achondrite NWA 7325 has the most positive $\delta^{49/47}$Ti value of all investigated samples with $\delta^{49/47}$Ti = 0.733 ± 0.060 (Fig. 2). Northwest Africa 7325 is a unique meteorite that likely originates from a so far unsampled parent body based on O and Cr isotope data and its unusual mineralogy (Barrat et al., 2015; Goodrich et al., 2017; Irving et al., 2013; Weber et al., 2016). Its O isotope composition overlaps with that of ureilites (Barrat et al., 2015; Goodrich et al., 2017; Irving et al., 2013; Weber et al., 2016), whereas its nucleosynthetic Cr and Ti isotope compositions are identical to acapulcoites (Goodrich et al., 2017). Northwest Africa 7325 was described as a medium-grained cumulate gabbro consisting of plagioclase (55–60%), diopside (25–30%), forsteritic olivine (10–16%) and accessories of sulphide, metal, chromite and eskolaite (Barrat et al., 2015; Goodrich et al., 2017; Irving et al., 2013). It appears to be a cumulate that formed from a largely basaltic melt, low in incompatible elements and Ti (Goodrich et al., 2017). In addition, NWA 7325 experienced secondary melting likely related to an impact followed by fast cooling (Yang et al., 2019). Based on valences of Ti, V and Cr in olivine and pyroxene (Sutton et al., 2017), it formed under highly reduced conditions. North West Africa 7325 was initially suggested to potentially originate from Mercury based on the presence of diopside that matched spectral observations of Mercury (Irving et al., 2013). However, NWA 7325 displays very old ages (4563.4 ± 2.6 Ma, Pb-Pb; 4563.10 ± 0.27, ^{26}Al-^{26}Mg relative to d'Orbigny) and therefore likely formed on an asteroidal body (Koefoed et al., 2016). Like NWA 7325, aubrites also display heavy $\delta^{49/47}$Ti values compared to the HED meteorites, but of a smaller magnitude than NWA 7325 (Fig. 2). As mentioned before, it was proposed that the Ti isotope composition of aubrites is due to reducing conditions during differentiation of aubrites that allowed for chalcophilic Ti^{3+} and lithophilic Ti^{4+} (Greber et al., 2017b). North West Africa 7325 also contains minor amounts of sulphides. Since Ti^{3+} occurs in olivine and pyroxene of NWA 7325, chalcophilic Ti^{3+} was likely also present on the parent body of NWA 7325. Therefore, sulphides could have contributed to the removal of isotopically light Ti for example, during the extraction of incompatible elements from the source of NWA 7325. However, the available data (Barrat et al., 2015; Goodrich et al., 2017; Yang et al., 2019) suggest that sulphides contain only a minor amount of Ti and that most Ti is hosted in the major silicate phases. Therefore, chalcophilic Ti^{3+}, if present in NWA 7325, likely had only a marginal effect on the $\delta^{49/47}$Ti of the bulk sample. The variable redox state of Ti (Ti^{3+} versus Ti^{4+}) in pyroxene of NWA 7325 (Sutton et al., 2017) could potentially lead to isotope fractionation behaviour, that is distinct from the terrestrial environment. For Earth, it has been shown that fractional crystallisation in ultramafic to mafic rocks do not lead to significant Ti isotope fractionation (Millet et al., 2016; Greber et al., 2017b; Deng et al., 2018a). Pyroxene is expected to dominate the Ti mass balance of NWA 7325 and has therefore a major leverage, if it fractionates Ti isotopes. Both pyroxene and olivine in NWA 7325 formed under highly reduced conditions and contain considerable amounts of Ti^{3+} in addition to Ti^{4+} (Sutton et al., 2017), the dominant redox state of Ti on Earth (Tillmanns and Correns, 1972; Waychunas, 1987). At equilibrium, lower oxidation states prefer light isotopes (Schauble, 2004) and therefore Ti^{3+} likely is enriched in light isotopes. This is consistent with theoretical Ti equilibrium fractionation factors determined using force constants and density functional theory (Wang et al., 2020). This work estimated that pyroxene containing pure Ti^{3+} has a lighter $\delta^{49/47}$Ti by ~0.9‰ compared to Ti^{4+}-pyroxene at 1000 K. Since NWA 7325 is described as a cumulate rock with pyroxene that formed from a largely basaltic melt, crystallising pyroxene with a light Ti composition will shift the $\delta^{49/47}$Ti of the cumulate towards light compositions. This is opposite to the observed heavy composition of NWA 7325. A light composition of pyroxene is also likely based on consideration of the Ti fractionation behaviour between melt and pyroxene using the coordination state of Ti. Pyroxene in NWA 7325 mainly contains 6-fold coordinated Ti with some minor (26%) 4-fold coordinated Ti (Sutton et al., 2017), whereas basaltic melts contain both 5-fold and 6-fold coordinated Ti (Farges and Brown Jr., 1997). Therefore, melt has in general a lower coordination number, when neglecting the 4-fold coordinated Ti. Lower coordination numbers are associated with stiffer bonds and enrichment of heavy isotopes (Schauble, 2004), therefore pyroxene is expected to be again enriched in isotopically light Ti compared to the melt. As pointed out above, this will lead to a light composition of NWA 7325 instead of the observed heavy one. Only in the case that 4-fold coordinated Ti in pyroxene dominates the system, isotopically heavy Ti by ~0.8‰ (at 1000 K) compared to 6-fold coordinated Ti (Leitzke et al., 2018) can be expected in pyroxene. However, to determine if this could be a viable scenario, further work on the coordination of Ti during pyroxene crystallisation in NWA 7325 is required. Iron-Ti oxides are in general considered to be isotopically light in Ti compared to melt and silicate phases based on existing models for magmatic Ti isotope fractionation (Deng et al., 2019; Greber et al., 2017a; Millet et al., 2016), equilibrium fractionation factors of oxide and silicate phases derived by density functional theory (Wang et al., 2020) and also based on Ti isotope data for ilmenite, magnetite and heavy mineral separates (Johnson et al., 2019; Mandl, 2019; He et al., 2020). Enrichments in isotopically heavy Ti ($\delta^{49/47}$Ti = 1.66 ± 0.05) have been documented for magnetite in a single case only, in mineral separates from a quartz monzonite (He et al., 2020). Based on this, it seems unlikely that the unusual formation of isotopically heavy oxides (magnesiochromite, ferrochromite, magnetite; Barrat et al., 2015; Irving et al., 2013; Weber et al., 2016) from the parent melt produced the heavy $\delta^{49/47}$Ti composition of NWA 7325. It is important to note that NWA 7325 is highly depleted in Ti, likely as a result of fractional crystallisation and melting under reducing conditions. This produced large positive Eu anomalies in the feldspar rich NWA 7325 and a depletion of incompatible elements, including Ti, in the source rock of NWA 7325 (Barrat et al., 2015). It is therefore conceivable that the Ti depletion event of the gabbroic or anorthositic source rock (Barrat et al., 2015; Frossard et al., 2019) produced the heavy $\delta^{49/47}$Ti composition of NWA 7325. In such a scenario, isotopically light Ti was retained by Fe-Ti oxides, which were not included into the source of NWA 7325. This led to the depletion of Fe and light Ti in the source and simultaneously enriched heavy Ti isotopes. These were then inherited by the melt forming NWA 7325. Additionally, NWA 7325 is rich in plagioclase (55–60%), which is anticipated to preferentially incorporate heavy isotopes based on Ti isotope data of plagioclase separates (He et al., 2020; Mandl, 2019). Preferential incorporation of isotopically heavy Ti into plagioclase is consequently likely to contribute partially to the heavy Ti isotope data of NWA 7325. This indicates that the high $\delta^{49/47}$Ti value of NWA 7325 has been produced by multiple fractionation events involving Fe-Ti oxides and plagioclase under reducing conditions. In summary, the new Ti isotope results provide evidence that nebular processes and accretion produced only small Ti isotope fractionation and suggest that different early solar system bodies have a uniform mass-dependent Ti isotope composition within reported uncertainties (2 standard deviations). In contrast, magmatic differentiation can produce Ti isotope fractionation on reduced parent-bodies as documented for NWA 7325, aubrites, the Moon and the Earth (Fig. 2; Deng et al., 2019; Greber et al., 2017a; Greber et al., 2017b; Kommescher et al., 2020; Millet et al., 2016).

6. Conclusions

The double spike technique was utilised for the determination of mass-dependent Ti isotope fractionation within terrestrial and meteorite samples using MC-ICP-MS and a new optimised three stage ion-exchange separation technique. Two single element laboratory standards (Ti Alfa Aesar solution and Ti Alfa Aesar wire), the OL-Ti standard and three terrestrial reference samples were analysed to test the methodologies. Mass-dependent Ti isotope data for two basaltic and one andesitic reference sample agree well with literature data and therefore verify the accuracy of the presented methodologies.

Our newly obtained mass-dependent Ti isotope data of two Rumuruti chondrites and the acapulcoite Dhofar 125 fall within the compositional range of ordinary and carbonaceous chondrites. Small mass-dependent Ti isotope variations are evident for different meteorite samples in this and also previous studies and seem unrelated to different meteorite groups and thermal metamorphism. Therefore, only limited mass-dependent Ti isotope fractionation is evident for early solar nebula or parent body processes for chondrites, eucrites and acapulcoites. Sample heterogeneity is likely responsible for at least part of the documented Ti isotope variations. Therefore, additional high-precision Ti isotope analyses of representative meteorite samples are necessary to further investigate about the cause for the spread in mass-dependent isotope compositions for chondrites and to verify that the Earth has a chondritic composition.

The unique ungrouped achondrite NWA 7325 displays larger Ti isotope variations compared to all investigated samples, which is likely related to magmatic processes that occurred under highly reducing conditions present on its parent body and/or oxide and plagioclase formation. A better understanding of Ti isotope fractionation processes under such unusual reduced conditions would help to further constrain the conditions of the NWA 7325 parent body.

Declaration of Competing Interest

The first author Niel H. Williams works since December 2019 for Thermo Fisher Scientific. Neptune and Neptune plus instruments were used for Ti isotope analyses of the presented study and Thermo Fisher Scientific is the manufacturer of those instruments. The main analytical work of this study was performed at the Open University using a Neptune instrument as part of the PhD thesis of Niel H. Williams (Williams, 2014, University of Manchester) – in addition, a standard comparison was measured on a Neptune Plus instrument at ETH Zürich (by M. B. Mandl). The authors declare that this relationship had no influence on the work that is reported in this paper.

The authors declare that they have no known competing financial interests or personal relationships that could have appeared to influence the work reported in this paper.

Acknowledgements

This work was supported by the Science and Technology Facilities Council (UK) in the form of a PhD studentship to N. H. Williams as well as the Swiss National Science Foundation. C. Davies, K. Theis and S. Hammond are thanked for their much appreciated laboratory support and W. Akram for providing the Ti sample aliquots. We thank the Natural History Museum in London (Caroline Smith), the Smithsonian Institution National Museum of Natural History (Linda Welzenbach), the Johnson Space Centre in Houston (Anne Kascak), the National Museum of Natural History in Paris (Brigitte Zanda), the Field Museum in Chicago (Philip Heck) for providing samples. We are also grateful to Anthony Irving for providing NWA 7325 and Addi Bischoff for the R-chondrites NWA 753 and NWA 755. We thank Marc-Alban Millet for providing us with an aliquot of the OL-Ti standard. Zhengbin Deng and Nicolas Greber are thanked for their constructive reviews and Catherine Chauvel for editor handling.

Appendix A. Supplementary data

Supplementary data to this article can be found online at https://doi.org/10.1016/j.chemgeo.2020.120009.

References

Akram, W., Schönbächler, M., Sprung, P., Vogel, N., 2013. Zirconium-hafnium isotope evidence from meteorites for the decoupled synthesis of light and heavy neutron-rich nuclei. Astrophys. J. 777, 169.

Akram, W., Schönbächler, M., Bisterzo, S., Gallino, R., 2015. Zirconium isotope evidence for the heterogeneous distribution of s-process materials in the solar system. Geochim. Cosmochim. Acta 165, 484–500.

Albalat, E., Telouk, P., Albarède, F., 2012. Er and Yb isotope fractionation in planetary materials. Earth Planet. Sci. Lett. 355-356, 39–50.

Alexander, C.M.O.D., Grossman, J.N., Ebel, D.S., Ciesla, F.J., 2008. The formation conditions of chondrules and chondrites. Science 320, 1617–1619.

Amsellem, E., Moynier, F., Pringle, E.A., Bouvier, A., Chen, H., Day, J.M.D., 2017. Testing the chondrule-rich accretion model for planetary embryos using calcium isotopes. Earth Planet. Sci. Lett. 469, 75–83.

Anbar, A.D., Roe, J.E., Barling, J., Nealson, K.H., 2000. Nonbiological fractionation of iron isotopes. Science 288, 126–128.

Arnold, T., et al., 2010. Measurement of zinc stable isotope ratios in biogeochemical matrices by double-spike MC-ICPMS and determination of the isotope ratio pool available for plants from soil. Anal. Bioanal. Chem. 398, 3115–3125.

Ayers, J.C., Watson, E.B., 1991. Solubility of apatite, monazite, zircon, and rutile in supercritical aqueous fluids with implications for subduction zone geochemistry. Phil. Trans. R. Soc. A 335, 365–375.

Ayers, J.C., Watson, E.B., 1993. Rutile solubility and mobility in supercritical aqueous fluids. Contrib. Mineral. Petrol. 114, 321–330.

Barrat, J.A., et al., 2015. Crustal differentiation in the early solar system: Clues from the unique achondrite Northwest Africa 7325 (NWA 7325). Geochim. Cosmochim. Acta 168, 280–292.

Binzel, R.P., Xu, S., 1993. Chips off of asteroid 4 Vesta: evidence for the parent body of basaltic achondrite meteorites. Science 9, 186–191.

Bischoff, A., Vogel, N., Roszjar, J., 2011. The Rumuruti chondrite group. Chem. Erde 71, 101–133.

Breton, T., Quitte, G., 2014. High-precision measurements of tungsten stable isotopes and application to earth sciences. J. Anal. At. Spectrom. 29, 2284–2293.

Burkhardt, C., Hin, R.C., Kleine, T., Bourdon, B., 2014. Evidence for Mo isotope fractionation in the solar nebula and during planetary differentiation. Earth Planet. Sci. Lett. 391, 201–211.

Burkhardt, C., et al., 2017. In search of the Earth-forming reservoir: Mineralogical, chemical, and isotopic characterizations of the ungrouped achondrite NWA 5363/NWA 5400 and selected chondrites. Meteorit. Planet. Sci. 52, 807–826.

Cameron, V., Vance, D., Archer, C., House, C.H., 2009. A biomarker based on the stable isotopes of nickel. Proc. Natl. Acad. Sci. 106, 10944–10948.

Creech, J.B., et al., 2017a. Late accretion history of the terrestrial planets inferred from platinum stable isotopes. Geochem. Perspect. Lett. 3, 94–104.

Creech, J.B., Moynier, F., Bizzarro, M., 2017b. Tracing metal–silicate segregation and late veneer in the Earth and the ureilite parent body with palladium stable isotopes. Geochim. Cosmochim. Acta 216, 28–41.

Dauphas, N., John, S.G., Rouxel, O., 2017. Iron Isotope Systematics, Non-traditional stable isotopes. Rev. Mineral. Geochem. 415–510.

Davis, A.M., Zhang, J., Greber, N.D., Hu, J., Tissot, F.L.H., Dauphas, N., 2018. Titanium isotopes and rare earth patterns in CAIs: evidence for thermal processing and gas-dust decoupling in the protoplanetary disk. Geochim. Cosmochim. Acta 221, 275–295.

Deng, Z., Moynier, F., Sossi, P.A., Chaussidon, M., 2018a. Bridging the depleted MORB mantle and the continental crust using titanium isotopes. Geochem. Perspect. Lett. 9, 11–15.

Deng, Z., Chaussidon, M., Savage, P., Robert, F., Pik, R., Moynier, F., 2019. Titanium isotopes as a tracer for the plume or island arc affinity of felsic rocks. Proc. Natl. Acad. Sci. 116, 1132–1135.

Deng, Z., Moynier, F., Van Zuilen, K., Sossi, P.A., Pringle, E.A., Chaussidon, M., 2018b. Lack of resolvable titanium stable isotopic variations in bulk chondrites. Geochim. Cosmochim. Acta 239, 409–419.

Duke, M.B., 1967. Petrology of eucrites, howardites and mesosiderites. Geochim. Cosmochim. Acta 31, 1637–1665.

Ek, M., Hunt, A.C., Lugaro, M., Schönbächler, M., 2020. The origin of s-process isotope heterogeneity in the solar protoplanetary disk. Nat. Astronom. 4, 273–281.

Farges, F., Brown Jr., G.E., 1997. Coordination chemistry of titanium(IV) in silicate glasses and melts: IV. XANES studies of synthetic and natural volcanic glasses and tektites at ambient temperature and pressure. Geochim. Cosmochim. Acta 61, 1863–1870.

Floyd, P.A., Winchester, J.A., 1978. Identification and discrimination of altered and metamorphosed volcanic rocks using immobile elements. Chem. Geol. 21, 291–306.

Frossard, P., Boyet, M., Bouvier, A., Hammouda, T., Monteux, J., 2019. Evidence for anorthositic crust formed on an inner solar system planetesimal. Geochem. Perspect. Lett. 11, 28–32.

Gall, L., Williams, H., Siebert, C., Halliday, A., 2012. Determination of mass-dependent variations in nickel isotope compositions using double spiking and MC-ICPMS. J. Anal. At. Spectrom. 27, 137–145.

Gault-Ringold, M., Stirling, C., 2012. Anomalous isotopic shifts associated with organic resin residues during cadmium isotopic analysis by double spike MC-ICPMS. J. Anal. At. Spectrom. 27, 449–459.

Georg, R.B., Halliday, A.N., Schauble, E.A., Reynolds, B.C., 2007. Silicon in the Earth's core. Nature 447, 1102–1106.

Gerber, S., Burkhardt, C., Budde, G., Metzler, K., Kleine, T., 2017. Mixing and transport of dust in the early solar nebula as inferred from titanium isotope variations among chondrules. Astrophys. J. 841, L17.

Goodrich, C.A., et al., 2017. Petrogenesis and provenance of ungrouped achondrite Northwest Africa 7325 from petrology, trace elements, oxygen, chromium and titanium isotopes, and mid-IR spectroscopy. Geochim. Cosmochim. Acta 203, 381–403.

Greber, N.D., Dauphas, N., Bekker, A., Ptàcek, M.P., Bindeman, I.N., Hofmann, A., 2017a. Titanium isotopic evidence for felsic crust and plate tectonics 3.5 billion years ago. Science 357, 1271–1274.
Greber, N.D., Dauphas, N., Puchtel, I.S., Hofmann, B.A., Arndt, N.T., 2017b. Titanium stable isotopic variations in chondrites, achondrites and lunar rocks. Geochim. Cosmochim. Acta 213, 534–552.
Haack, H., et al., 2019. Ejby-a new H5/6 ordinary chondrite fall in Copenhagen, Denmark. Meteorit. Planet. Sci. 54, 1853–1869.
He, X., Ma, J., Wei, G., Zhang, L., Wang, Z., Wang, Q., 2020. A new procedure for titanium separation in geological samples for $^{49}Ti/^{47}Ti$ ratio measurement by MC-ICP-MS. J. Anal. At. Spectrom. 35, 100–106.
Hezel, D.C., Russell, S.S., Ross, A.J., Kearsley, A.T., 2008. Modal abundances of CAIs: Implications for bulk chondrite element abundances and fractionations. Meteorit. Planet. Sci. 43, 1879–1894.
Hin, R.C., et al., 2017. Magnesium isotope evidence that accretional vapour loss shapes planetary compositions. Nature 549, 511–515.
Hoare, L., Klaver, M., Saji, N.S., Gillies, J., Parkinson, I.J., Lissenberg, C.J., Millet, M.-A., 2020. Melt chemistry and redox conditions control titanium isotope fractionation during magmatic differentiation. Geochim. Cosmochim. Acta 282, 38–54.
Hopp, T., Kleine, T., 2018. Nature of late accretion to Earth inferred from mass-dependent Ru isotopic compositions of chondrites and mantle peridotites. Earth Planet. Sci. Lett. 494, 50–59.
Huang, S., Jacobsen, S.B., 2017. Calcium isotopic compositions of chondrites. Geochim. Cosmochim. Acta 201, 364–376.
Huang, S., Farkas, J., Yu, G., Petaev, M.I., Jacobsen, S.B., 2012. Calcium isotopic ratios and rare earth element abundances in refractory inclusions from the Allende CV3 chondrite. Geochim. Cosmochim. Acta 77, 252–265.
Huss, G.R., Rubin, A.E., Grossman, J.N., 2006. Thermal metamorphism in chondrites. In: Lauretta, D.S., McSween Jr., H.Y. (Eds.), Meteorites and the Early Solar System II. University of Arizona Press, Tucson, pp. 567–586.
Hutchison, R., 2004. Meteorites: A Petrologic, Chemical and Isotopic Synthesis. Cambridge Planetary Science, 506 pp.
Ireland, T.R., Zinner, E.K., Fahey, A.J., Esat, T.M., 1992. Evidence for distillation in the formation of HAL and related hibonite inclusions. Geochim. Cosmochim. Acta 56, 2503–2520.
Irving, A.J., et al., 2013. Ungrouped mafic achondrite Northwest Africa 7325: a reduced, iron-poor cumulate olivine gabbro from a differentiated planetary body. Lunar Planet. Sci. 44, 2164.
Jarosewich, E., 1990. Chemical analyses of meteorites: a compilation of stony and iron meteorite analyses. Meteoritics 25, 323–337.
Jochum, K.P., et al., 2016. Reference values following ISO guidelines for frequently requested rock reference materials. Geostand. Geoanal. Res. 40, 333–350.
Johnson, A.C., et al., 2019. Titanium isotopic fractionation in Kilauea Iki lava lake driven by oxide crystallization. Geochim. Cosmochim. Acta 264, 180–190.
Keil, K., McCoy, T.J., 2018. Acapulcoite-lodranite meteorites: ultramafic asteroidal partial melt residues. Geochemistry 78, 153–203.
Klaver, M., Ionov, D.A., Takazawa, E., Elliott, T., 2020. The non-chondritic Ni isotope composition of Earth's mantle. Geochim. Cosmochim. Acta 268, 405–421.
Koefoed, P., Amelin, A., Yin, Q.-Z., Wimpenny, J., Sanborn, M.E., Iizuka, T., Irving, A.J., 2016. U–Pb and Al–Mg systematics of the ungrouped achondrite Northwest Africa 7325. Geochim. Cosmochim. Acta 183, 31–45.
Kommescher, S., Fonseca, R.O.C., Kurzweil, F., Thiemens, M.M., Münker, C., Sprung, P., 2020. Unravelling lunar mantle source processes via the Ti isotope composition of lunar basalts. Geochem. Perspect. Lett. 13, 13–18.
Krabbe, N., Kruijer, T., Kleine, T., 2017. Tungsten stable isotope compositions of terrestrial samples and meteorites determined by double spike MC-ICPMS. Chem. Geol. 450, 135–144.
Leitzke, F.P., Fonesca, R.O.C., Göttlicher, J., Steininger, R., Jahn, S., Prescher, C., Lagos, M., 2018. Ti K-edge XANES study on the coordination number and oxidation state of titanium in pyroxene, olivine, armalcolite, ilmenite, and silicate glass during mare basalt petrogenesis. Contrib. Mineral. Petrol. 173, 103.
Leya, I., Schönbächler, M., Wiechert, U., Krähenbühl, U., Halliday, A.N., 2007. High precision titanium isotopic measurements on geological samples by high resolution MC-ICPMS. Int. J. Mass Spectrom. 262, 247–255.
Leya, I., Schönbächler, M., Wiechert, U., Krahenbühl, U., Halliday, A.N., 2008. Titanium isotopes and the radial heterogeneity of the solar system. Earth Planet. Sci. Lett. 266, 233–244.
Leya, I., Schönbächler, M., Krähenbühl, U., Halliday, A.N., 2009. New titanium isotope data for Allende and Efremovka CAIs. Astrophys. J. 702, 1118–1126.
MacPherson, G.J., Wark, D.A., Armstrong, J.T., 1988. Primitive material surviving in chondrites: refractory inclusions. In: Kerridge, J.F., Matthews, M.S. (Eds.), Meteorites and the Early Solar System. University of Arizona Press, Tucson.
Mandl, M.B., 2019. Titanium Isotope Fractionation on the Earth and Moon: Constraints on Magmatic Processes and Moon Formation. Doctoral Thesis. ETH Zürich.
McCoy-West, A.J., Millet, M.-A., Burton, K.W., 2017. The neodymium stable isotope composition of the silicate Earth and chondrites. Earth Planet. Sci. Lett. 480, 121–132.
Millet, M.-A., Dauphas, N., 2014. Ultra-precise titanium stable isotope measurements by double-spike high resolution MC-ICP-MS. J. Anal. At. Spectrom. 29, 1444–1458.
Millet, M.-A., et al., 2016. Titanium stable isotope investigation of magmatic processes on the Earth and Moon. Earth Planet. Sci. Lett. 449, 197–205.
Mittlefehldt, D.W., McCoy, T.J., Goodrich, C.A., Kracher, A., 1998. Non-chondritic meteorites from asteroidal bodies. In: Papike, J.J. (Ed.), Planetary Materials. Reviews in Mineralogy. Mineral. Soc. Am., p. 195
Murphy, K., Rehkämper, M., Kreissig, K., Coles, B., Van de Flierdt, T., 2016. Improvements in Cd stable isotope analysis achieved through use of liquid–liquid extraction to remove organic residues from Cd separates obtained by extraction chromatography. J. Anal. At. Spectrom. 31, 319–327.
Niederer, F.R., Papanastassiou, D.A., 1984. Ca isotopes in refractory inclusions. Geochim. Cosmochim. Acta 48, 1279–1293.
Niederer, F.R., Papanastassiou, D.A., Wasserburg, G.J., 1981. The isotopic composition of titanium in the Allende and Leoville meteorites. Geochim. Cosmochim. Acta 45, 1017–1031.
Niederer, F.R., Papanastassiou, D.A., Wasserburg, G.J., 1985. Absolute isotopic abundances of Ti in meteorites. Geochim. Cosmochim. Acta 49, 835–851.
Palme, H., Schulz, L., Spettel, B., Weber, H.W., Wänke, H., Christophe Michel-Levy, M., Lorin, J.C., 1981. The Acapulco meteorite: chemistry, mineralogy and irradiation effects. Geochim. Cosmochim. Acta 727-729, 743–752.
Patzer, A., Hill, D.H., Boynton, W.V., 2004. Evolution and classification of acapulcoites and lodranites from a chemical point of view. Meteorit. Planet. Sci. 39, 61–85.
Pearce, J.A., Norry, M.J., 1979. Petrogenetic implications of Ti, Zr, Y, and Nb variations in volcanic rocks. Contrib. Mineral. Petrol. 69, 33–47.
Righter, K., Sutton, S.R., Danielson, L., Pando, K., Newville, M., 2016. Redox variations in the inner solar system with new constraints from vanadium XANES in spinels. Am. Mineral. 101, 1928–1942.
Ripperger, S., Rehkämper, M., 2007. Precise determination of cadmium isotope fractionation in seawater by double spike MC-ICPMS. Geochim. Cosmochim. Acta 71, 631–642.
Rudge, J.F., Reynolds, B.C., Bourdon, B., 2009. The double spike toolbox. Chem. Geol. 265, 420–431.
Saji, N.S., Wielandt, D., Paton, C., Bizzarro, M., 2016. Ultra-high-precision Nd-isotope measurements of geological materials by MC-ICPMS. J. Anal. At. Spectrom. 31, 4190-1504.
Schauble, E.A., 2004. Applying stable isotope fractionation theory to new systems, Geochemistry of Non-Traditional Stable Isotopes. In: Reviews in Mineralogy & Geochemistry. Mineral. Soc. Am., pp. 65–111
Schönbächler, M., Rehkämper, M., Lee, D.-C., Halliday, A.N., 2004. Ion exchange chromatography and high precision isotopic measurements of zirconium by MC-ICPMS. Analyst 129, 32–37.
Schönbächler, M., Carlson, R.W., Horan, M.F., Mock, T.D., Hauri, E.H., 2007. High precision Ag isotope measurements in geological materials by multiple-collector ICPMS: an evaluation of dry versus wet plasma. Int. J. Mass Spectrom. 261, 183–191.
Shima, M., 1979. The abundances of titanium, zirconium and hafnium in stony meteorites. Geochim. Cosmochim. Acta 43, 353–362.
Siebert, C., Nägler, T.F., Kramers, J.D., 2001. Determination of molybdenum isotope fractionation by double-spike multicollector inductively coupled plasma mass spectrometry. Geochem. Geophys. Geosyst. 2. No 2000GC000124.
Simon, J.I., DePaolo, D.J., 2010. Stable calcium isotopic composition of meteorites and rocky planets. Earth Planet. Sci. Lett. 289, 457–466.
Simon, S.B., Sutton, S.R., Grossman, L., 2016. The valence and coordination of titanium in ordinary and enstatite chondrites. Geochim. Cosmochim. Acta 189, 377–390.
Sutton, S.R., Goodrich, C.A., Wirick, S., 2017. Titanium, vanadium and chromium valences in silicates of ungrouped achondrite NWA 7325 and ureilite Y-791538 record highly-reduced origins. Geochim. Cosmochim. Acta 204, 313–330.
Teng, F.-Z., Dauphas, N., Watkins, J.M., 2017. Non-traditional stable isotopes: Retrospective and prospektive. In: Non-traditional Stable Isotopes. Reviews in Mineralogy & Geochemistry, pp. 1–26.
Tillmanns, E., Correns, C.W., 1972. Titanium. In: Wedepohl, K.H. (Ed.), Handbook of Geochemistry. Springer.
Trinquier, A., Elliott, T., Ulfbeck, D., Coath, C., Krot, A.N., Bizzarro, M., 2009. Origin of nucleosynthetic isotope heterogeneity in the solar protoplanetary disk. Science 324, 374–376.
Valdes, M.C., Moreira, M., Foriel, J., Moynier, F., 2014. The nature of Earth's building blocks as revealed by calcium isotopes. Earth Planet. Sci. Lett. 394, 135–145.
Wang, W., Huang, S., Huang, F., Zhao, X., Wu, Z., 2020. Equilibrium inter-mineral titanium isotope fractionation: Implication for high-temperature titanium isotope geochemistry. Geochim. Cosmochim. Acta 269, 540–553.
Waychunas, G.A., 1987. Synchrotron radiation XANES spectroscopy of Ti in minerals; effects of Ti bonding distances, Ti valence, and site geometry on absorption edge structure. Am. Mineral. 72, 89–101.
Weber, I., et al., 2016. Cosmochemical and spectroscopic properties of Northwest Africa 7325-a consortium study. Meteorit. Planet. Sci. 51, 3–30.
Williams, N.H., 2014. Titanium Isotope Cosmochemistry. PhD Thesis. University of Manchester.
Wood, B.J., Smythe, D.J., Harrison, T., 2019. The condensation temperatures of the elements: a reappraisal. Am. Mineral. 104, 844–856.
Yanai, K., Kojima, H., Haramura, H., 1995. Catalog of the Antarctic Meteorites Collected from December 1969 to December 1994, With Special Reference to those Represented in the Collections of the National Institute of Polar Research. National Institut of Polar Research.
Yang, J., Zhang, C., Miyahara, M., Tang, X., Gu, L., Lin, Y., 2019. Evidence for early impact on a hot differentiated planetesimal from Al-rich micro-inclusions in ungrouped achondrite Northwest Africa 7325. Geochim. Cosmochim. Acta 258, 310–335.
Zambardi, T., Poitrasson, F., Corgne, A., Méheut, M., Quitté, G., Anand, M., 2013. Silicon isotope variations in the inner solar system: Implications for planetary formation, differentiation and composition. Geochim. Cosmochim. Acta 121, 67–83.
Zhang, J., Dauphas, N., Davis, A.M., Pourmand, A., 2011. A new method for MC-ICPMS measurement of titanium isotopic composition: Identification of correlated isotope anomalies in meteorites. J. Anal. At. Spectrom. 26, 2197–2205.

Zhang, J.Z., Dauphas, N., Davis, A.M., Leya, I., Fedkin, A., 2012. The proto-Earth as a significant source of lunar material. Nat. Geosci. 5, 251–255.
Zhang, J., Huang, S., Davis, A.M., Dauphas, N., Hashimoto, A., Jacobsen, S.B., 2014. Calcium and titanium isotopic fractionations during evaporation. Geochim. Cosmochim. Acta 140, 365–380.
Zinner, E., 2014. 1.4 - Presolar grains. In: Holland, H.D., Turekian, K.K. (Eds.), Treatise on Geochemistry, Second edition. Elsevier, Oxford, pp. 181–213.